CAMBRIDGE
UNIVERSITY PRESS

CONFERENCE PAPER

Accessing old carbon influence on TOC ^{14}C age and environmental change from the recent sediments in Lake Shira, Russia

Satabdi Misra[1#], Dilyara Kuzina[2#], Tzu-Tsen Shen[1], Chun-Yen Chou[1], Anastasiya Yusupova[2], Pavel Krylov[2], Danis Nurgaliev[2] and Hong-Chun Li[1,3]

[1]Department of Geosciences, National Taiwan University, Taipei 10617, Taiwan, ROC, [2]Department of Geophysics and Geoinformation Technologies, Kazan (Volga Region) Federal University, Kazan 420008, Russia and [3]Frontiers Science Center for Deep Ocean Multispheres and Earth System, and Key Laboratory of Marine Chemistry Theory and Technology, Ministry of Education, Ocean University of China, Qingdao, China
Corresponding author: Hong-Chun Li; Email: hcli1960@ntu.edu.tw

Abstract

We present 35 AMS ^{14}C dates from 26 horizons on a 30-cm gravity core from Shira Lake in the republic of Khakassia, Central Russia. The chronology of the core is determined by ^{210}Pb/^{137}Cs dating results and interpretation of elemental geochemistry with historic documents, covering deposition since ca. 1870 CE. This study assesses the old carbon influence (OCI) on organic carbon ^{14}C by comparison with the ^{210}Pb/^{137}Cs dates, sources of carbon, and lake conditions interpreted from elemental proxies. These include elemental concentrations in 0.5N HCl leaches and Aqua Regia dissolution fractions, as well as organic C, N and C/N measurements. From these data we establish a succession of the following six zones: I) (1870~1900 CE) relatively fresh lake with high lake level, low productivity and high surface runoff (wet conditions); II) (1900~1940 CE) a "white zone" reflected by high carbonate and low magnetic signal formed in a saline, oxidizing and holomictic lake stage; III) (1940~1963 CE) reduced carbonate with elevated organic C, N, C/N, Mo and magnetic signal, indicating a stratified and anaerobic lake; IV) (1963~1994 CE) increased salinity and productivity with the highest observed magnetic signal and elevated heavy metal and Mo contents, implying enhanced anoxic conditions and human impact; V) (1994~2003 CE) high C/N, organic and carbonate contents suggesting meromictic and anaerobic lake conditions; VI) (2003~2020 CE) decreased carbonate content with increased organic C and N, and heavy metals showing a deteriorating lake environment under human impact.

Introduction

High-resolution multi-proxy records from accumulated sediments at the bottom of lakes are useful archives for reconstructing palaeoclimate and palaeoenvironmental changes (Chappell 1999; Chen et al. 2006; Hausmann et al. 2011; Lan et al. 2018; Owen et al. 1990; Smol and Cumming 2000). These sediments contain a variety of physical, geochemical, and biological proxy indicators that can be used to gain a multi-faceted understanding of past conditions. Lake sediments generally offer continuous high-resolution records of environmental change over thousands of years or longer in comparison to tree ring, coral and speleothem records. Although lakes are complex environmental systems and lake sediment

---

# These authors have contributed equally to this work and share the first authorship.

proxies can be challenging to interpret, lake-derived proxies have provided critical context for human-induced climate change in regions like the Arctic where instrumental observations are sparse and short in duration (Kaufman et al. 2009).

Sedimentation history from saline lakes reflect environmental changes in the catchment area. Climate change studies in south-central Russia are ideal for understanding the Westerly, Polar Easterly and Siberian High through time not only because of their geographical position (Figure 1) but also given the abundance of potential proxies for climate reconstruction (Schwikowski et al. 2009). The climate variation of this area during the Holocene has been previously reconstructed from numerous proxies such as tree rings (Dulamsuren et al. 2014; Myglan et al. 2012), palaeosols (Fedeneva and Dergacheva 2003), lake levels (Grunert et al. 2000), glacial geomorphology (Agatova et al. 2012; Blyakharchuk et al. 2008; Ganyushkin et al. 2018; Herren et al. 2013; Schlütz and Lehmkuhl 2007), clastic sediment properties (Kalugin et al. 2005), and biological indicators such as diatoms (Westover et al. 2006) and pollen (Blyakharchuk et al. 2017; Huang et al. 2018; Rudaya and Li 2013; Unkelbach et al. 2018). Chen et al. (2015) summarized the moisture conditions during the Medieval Warm Period (MWP) and the Little Ice Age (LIA). However, different parts of the mountain range experienced a different climate development in terms of temperature and humidity during the last 11,000 years owing to its significant topographic elevation. Ten detailed lake records in southern Russia are available: Teletskoye Lake (Andreev et al. 2007; Kalugin et al. 2007; Rudaya et al. 2016), Manzherok Lake (Blyakharchuk et al. 2017, 2020), Achit Nuur Lake (Sun et al. 2013), Hoton-Nur Lake (Rudaya and Li 2013), Shira Lake (Dar'in et al. 2015; Kalugin et al. 2013), Uzunkol, Taskol and Kendegelukol Lakes (Blyakharchuk et al. 2004), Grusha Lake, Akkol Lake (Blyakharchuk et al. 2007). Among those ten lake records, only Manzherok Lake and Shira Lake have detailed chronological control.

Lake Shira is situated in the semi-arid climatic area of South Siberia (Kalugin et al. 2013); particularly within the southern part of the Chebako-Balakhtinskaya basin (Dar'in et al. 2013). Lake Shira contains brackish water fed only by the Son river and does not have any outlet. Currently, the lake is often stratified and switches between meromictic and holomictic statuses (Barkhatov et al. 2022; Belolipetskii et al. 2017; Rogozin et al. 2010). The adjacent fresh water Lake Itkol is located 3.8 km west of and 100 m above Lake Shira (Kalugin et al. 2013). Limnological, physical, chemical and biological properties of Lake Shira have been extensively studied since 1999 (Dar'in et al. 2015; Degermendzhy et al. 2010; Kalacheva et al. 2002; Kalugin et al. 2013; Parnachev and Degermendzhy 2002; Rogozin et al. 2016b, 2020; Tretyakov et al. 2012; Zotina et al. 1999). Kalugin et al. (2013) established the chronology of a 20-cm box core (namely Shira 2010) by ^{137}Cs dating, varve counting and Ca/Sr variation, and the chronology of a 155-cm hammer core (namely Shira 2009) with three ^{14}C ages and varve counting in various depths. Dar'in et al. (2015, the report in Russian was in 2013) presented nine more ^{14}C ages in Core Shira 2009. Those ^{14}C ages were probably dated on bulk carbon (including both organic carbon and carbonate), showing strongly old carbon influence (OCI). Kalugin et al. (2013) and Dar'in et al. (2015) made corrections to the ^{14}C ages by subtracting 1200 or 1275 years. They attributed the "radiocarbon reservoir effect" to the carbonate formation in the lake associated with the inflow of ancient carbon from carbonate strata in the catchment area into the lake water. Several studies (e.g., Rogozin et al. 2016b, 2020) have adopted this chronology.

Precise radiocarbon dates have a crucial role in ascertaining a reliable chronology (Björck et al. 2002; Zhou et al. 2021) which connects different sediment depths to their ages through a numerical age-depth model such as the Bacon Model (Blaauw and Christen 2011). However, old carbon in lake sediments has a significant role in imparting a "radiocarbon reservoir effect" (Ojala et al. 2019). In general, the ^{14}C dating of lake sediments needs to go through proper sample treatments, such as acid-base-acid (ABA) treatment to remove carbonate and isolate organic carbon. But, even if the lake sediment sample is subjected to acid pretreatment to remove carbonates, multiple factors can still influence the natural content of ^{14}C in organic matter. For example, if aquatic plants and algae use dissolved CO_2 which contains old carbon for photosynthesis, the produced organic composition may contain OCI (Chen et al. 2021; Misra et al. 2024). In addition, soil organic carbon input into lakes by surface runoff can bring OCI for lake sediments. The above organic carbon is difficult to remove by ABA treatment. As ^{210}Pb
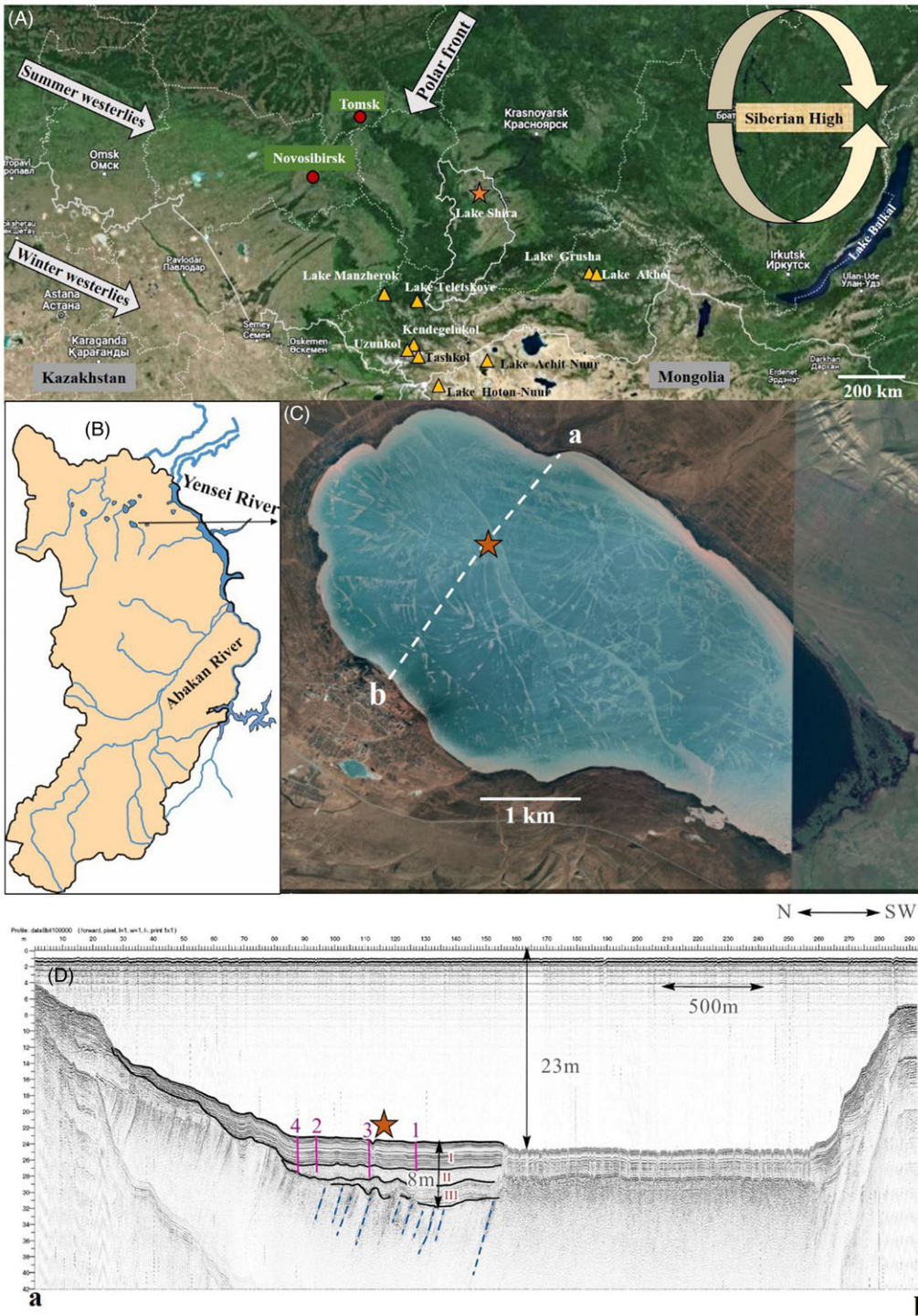
Figure 1. *Location of the study area. (A) map showing the location of Lake Shira (orange star) in the Republic of Khakassia in Southern Russia with nearby previously studied lake locations. The yellow triangles indicate the studied lakes in the area. (B) map showing the Republic of Khakassia and the location of Lake Shira. (C) satellite map of Lake Shira with the location of the core. (D) seismic map with coring sites of Lake Shira along the profile a-b.*

and ^{137}Cs dating methods are not able to date lake sediment cores older than 200 years, and lamination counting is not an absolute dating method, ^{14}C dating is probably the only choice for determining >200-year chronology. This raises two questions: (1) why does OCI exist in the ^{14}C ages of sedimentary organic carbon in Lake Shira? And (2) what is the best way to obtain a useful ^{14}C chronology of a sediment core from such a lake? This study attempts to answer these questions.

The present study combines high-resolution ^{14}C dating with ^{210}Pb and ^{137}Cs dating on a 30 cm long gravity core. To understand the effect of OCI on the ^{14}C dating of lake sediment total organic carbon (TOC), both acid (A) and acid-base-acid (ABA) treatments were applied to the samples from the same horizons for the removal of any impurities particularly carbonates. Elemental concentrations in the 0.5N HCl leach fraction (AL) and Aqua Regia dissolution fraction (AR) measured by an Inductively Coupled Plasma Optical Emission Spectrometry (ICPOES) and organic C, N, H and C/N measured by an Elemental Analyzer (EA) have been performed on the core with resolution of 1-cm interval. Magnetic susceptibility (MSus) of every cm of the core has been measured to understand the forcing factors of lake sediment MSus. The purpose of the present research is to provide a multi-proxy comprehensive record of Lake Shira for reconstructing lake conditions revealed in the 30-cm sediment core (about 200 years).

Study area and regional setting

Lake Shira (54°30′38″N, 90°12′09′E) is situated in the southern part of North-Minusinsk Depression in the republic of Khakassia, Central Russia and positioned approximately 355 m above sea level. The lake is confined to a drainless depression within the Shirinsky denudation-accumulative subplain. Shira is one of the large lakes of Northern Khakassia, which formed in a deflation basin on the site of synclinal structures (Vasilev and Parnachev 2006). Lake Shira has a length of about 9.4 km and a maximum width of 5 km (Figure 1). The lake area covers around 39 km². The water depth reaches 24 m in the central part (Degermendzhy et al. 2010; Kalugin et al. 2013). Along the lake shore, there are four abrasion terraces: with the height of the first above the modern lake water level is 3 m, the second is 4 m, the third is 10 m and the fourth is 14 m, indicating strong fluctuations in the water level in the past which is a closed lake feature (Ivankin 1979).

Lake Shira is regarded as a saline meromictic lake (i.e. multiple layers of water do not mix) without outflow (Figure S1) (Genova et al. 2010). The Son River flows into the lake from the southeast and delivers approximately 50% of the freshwater supply (Rogozin et al. 2010). Atmospheric precipitation and seepage water provide the other half of the water supply (Hildebrandt et al. 2015). The absence of the surface outflow is the most obvious reason for the saline meromictic nature of Lake Shira and the high salinity is documented in earlier studies (Belolipetsky et al. 2010; Genova et al. 2010; Rogozin et al. 2010). The water stratification is prominent during summer and this acts as a barrier restricting vertical mixing (Belolipetsky et al. 2010). Consequently, the upper water layer (mixolimnion; characterized by comparatively higher temperature and lower density) is unable to mix with persistent cold and dense water layers (Figure S1). However, deep mixing of the lake water occurred during the last month of 2014, and this transformed the nature of Lake Shira from meromictic to holomictic (Barkhatov et al. 2022; Belolipetskii et al. 2017; Rogozin et al. 2017). Hence, the stratification of Lake Shira varies with time under the influence of lake chemistry and climatic conditions.

Modern weather conditions in the studied area have been monitored with meteorological stations. The annual air temperature record at Barnaul since 1838 CE shows that before 1900 the temperature fluctuated between –2.4 and 3°C, then fluctuated between 0 and 3°C during 1900~1960 (data from the Siberian Branch of the Russian Academy of Science). The temperature increased significantly after 1960, and a warming trend is also shown in the temperature records of Minusinsk and Abakan. The study site experiences an average annual temperature of about 1 °C with an annual precipitation of 310–350 mm/yr. The rainy season is from May to September and the snowy season is from October to April. The surface of Lake Shira is expected to be frozen for seven months annually.

Methodology

Collection of samples

A 30-cm-long gravity core with a clear water-sediment interface was collected from Lake Shira in 2020 by the Russian team of Kazan Federal University (KFU). The core was further subsampled to 1-cm intervals in the field for a high-resolution palaeoclimatic reconstruction. Samples were thereafter sealed in plastic bags and stored in a refrigerator at 4°C in the laboratory for subsequent pre-treatment and experimental analyses. The samples were freeze-dried in the laboratory at KFU and separated into aliquots for AMS ^{14}C dating, gamma spectrometry counting and magnetic, geochemical and biological studies.

Gamma spectrometry measurements

Natural (^{210}Pb, ^{238}U, ^{226}Ra, ^{214}Pb, ^{232}Th, ^{214}Bi and ^{40}K) and artificial (^{137}Cs) radionuclide concentrations were measured using an ORTEC low-background semiconductor gamma spectrometer combined with a 10-cm thick low background lead shield with high purity germanium (HPGe) detector combined with a DSPEC LF digital analyser and Maestro-32 and Gamma-Vision-32 software at NTUAMS laboratory, Department of Geosciences, National Taiwan University (NTU), Taiwan.

The freeze-dried samples (all sample amount was used for the non-destructive measurement, weight ranges from 1.126 g to 5.263 g) were crushed to a particle size of less than 63 μm and then placed into a 6 cm-diameter container for gamma counting. The counting samples were carefully sealed and kept for at least 14 days to achieve the equilibrium state of the members of the ^{238}U decay series. Background measurements were conducted with a blank Marinelli vessel at the gamma spectrometer. The counting efficiency, geometry and density effects of the detector were calibrated by various standards (IAEA-446, IAEA-447 and IAEA-RG-Th-1). The sample container was placed on top of the detector. The energy of ^{210}Pb, ^{238}U, ^{226}Ra, ^{214}Pb, ^{232}Th, ^{214}Bi, ^{137}Cs and ^{40}K peaks in the gamma spectrometer were measured at 46.2 keV, 92 keV, 186 keV, 353 keV, 583 keV, 610 keV, 658 keV and 1464 keV, respectively. Supported ^{210}Pb activity was determined by the ^{226}Ra activity (using ^{214}Pb activity at 353 keV) in the sample measurements. The excess ^{210}Pb (^{210}Pb$_{ex}$) activity was calculated as the total ^{210}Pb activity less the supported ^{210}Pb activity. The gamma counting in the gamma spectrometer has less than ± 5% errors at the 95% confidence level. The ^{210}Pb chronology assumed a constant rate of supply model (Appleby and Oldfield 1992).

Acid-leachable (AL) elemental analysis by ICP-OES

A total of 29 samples (the surface 1 cm sample was used up for other analyses) of the core were used for these analyses. Around 300 mg of each sample was taken and placed into a 50 mL centrifuge tube and leached by a 15 mL 0.5N HCl solution. This process is advantageous for the elimination of inorganic carbon (mainly carbonate impurities) and absorbed oxides on the particle surface. Moreover, this procedure does not affect organic components and detrital phases in the sediments. The acid-leachable elements are considered as an active portion which reflects chemical conditions and productivity in the water column (Li et al. 2022). After centrifugation, the acid solution was fixed to 50 mL with a volumetric flask. Then, the sample solution was measured by a PerkinElmer (PE) Optima 8000DV ICP-OES in the NTUAMS Lab. Seventeen elements (Ca, Mg, Fe, Al, Mn, K, Cu, Ni, Ba, Zn, Pb, Sr, Rb, Ti, Cr, Mo and U) were selected for the analysis. The elemental concentrations measured by ICP-OES were calculated by the standard curves of different elements at various concentrations of standard solutions. The correlation coefficient (R^2) of the intensity-concentration relationship for each element is normally greater than 0.98. The uncertainty of the measurement is about 0.2% for 1 mg/L (ppm) level.

The residue after the acid-leachable elemental analysis was divided into three fractions for analyses: (1) ^{14}C AMS dating (approximately 45 mg); (2) organic C, N, H, S analysis by EA (approximately 20 mg); and (3) aqua regia digested elements (approximately 100 mg).

CHNS by Element Analyzer (EA)

Total organic carbon (C), nitrogen (N), hydrogen (H) and sulphur (S) were obtained using a Thermo Scientific Flash 2000 Elemental analyzer (EA). Approximately 20 mg of each sample was placed into a small tin cup and loaded into an autosampler. The sample was combusted in the quartz tube with O_2 at 950 °C. The gas liberated was further reacted with tungsten oxide to deliver additional oxygen to catalyse the complete combustion of the sample and prevent the formation of non-volatile sulphates. The produced gases were then reacted with electrolytic copper for a reduction mechanism. The elemental analyzer was calibrated by a 2,5-Bis(5-tert-butyl-2-benzo-oxazol-2-yl) thiophene (BBOT) standard and the standard was measured in every five samples.

Elemental analysis of elements dissolved in aqua regia (AR) by microwave digestion

Approximately 100 mg of sample from every 1 cm depth horizon were weighed and subsequently digested with AR which is a mixture of concentrated nitric (HNO_3) and hydrochloric (HCl) acids (1 mL of HNO_3 + 3 mL of HCl). The digestion was performed in a polytetrafluoroethylene tube and placed in a ceramic holder for a Anton Paar Multiwave 3000 microwave system at the NTUAMS Lab. The microwave program ran for 15 minutes at about 145°C, for 20 minutes at 200°C, and a holding time of 15 minutes, followed by a cooling procedure of 10 minutes. After the microwave digestion, the acid solution was filtered through an acetate filter membrane with 0.45-µm pore size to remove any undissolved particles. The filtered solution was analysed for 17 elements, the same as for the AL elements using the ICP-OES at the NTUAMS Lab.

AMS ^{14}C dating

Accelerator mass spectrometry (AMS) ^{14}C dating was performed in the NTUAMS Lab with a HVE 1.0 MV Tandetron Model 4110 BO AMS. A total of 35 AMS ^{14}C dates were measured from the core in three batches. The first batch contained 7 samples (Lab codes in 7300 and 7400 series in Table 1) were measured in April and August 2021. Those samples were from the original samples and treated with an acid-base-acid (ABA) treatment following the description in Misra et al. (2024). The second batch containing 19 samples was conducted in December 2022 and February 2023. Those samples were the residues after acid-leach sediments (after the procedure mentioned in 3.3.). The third batch containing 9 samples was analysed in November 2023. For the 3rd batch of samples, we performed both A- and ABA-treatment for comparison. All A- or ABA-treated samples of about 30 mg were placed into a 9-mm diameter quartz tube for TOC ^{14}C dating. About 75 mg of CuO and a small piece of silver wire were added to the quartz tube. The tube was placed onto the vacuum line to pump out the air. When the vacuum of the tube reached 5×10^{-6} mbar, the tube was taken off the line and sealed under 1400ºC. The sealed tube was placed into a muffle furnace for 8 hours to combust at 850°C. The TOC in the sediments was oxidized into CO_2. The produced CO_2 was purified and transferred into graphite for AMS measurement following the description of Li et al. (2022).

Magnetic analysis

Magnetic bulk susceptibility was measured for all 30 samples of Shira GC4 with a 1-cm sampling interval in the Magnetic Lab at Kazan (Volga Region) Federal University (KFU). Each sample was placed into a plastic sample holder and measured by Kappabridge equipment (model MFK-1A, AGICO-Czech Republic) at room temperature. All measurements were adjusted to sample weight. The operating frequency of the machine is 976 Hz with 5×10^{-8} m³/kg sensitivity.

Table 1. *AMS ^{14}C dates of Shira GC4. Lab code has the NTUAMS prefix*

Lab code	Sample ID	Depth (cm)	Treat-ment	F_S	^{14}C age (yr BP)	#Year (CE)	F_{atm}	ΔT (years)
−8416*	−2-c	1.5	A	0.9938 ± 0.0063	50 ± 51	2013	1.0050 ± 0.0043	115
−8417*	−3-a	2.5	A	1.0106 ± 0.0065	−85 ± 51	2009	1.0580 ± 0.0065	
−7303-1	−4	3.5	ABA	1.0006 ± 0.0097	−5 ± 78	2004	1.0742 ± 0.0017	
−8418*	−5-a	4.5	A	1.0218 ± 0.0065	−173 ± 51	1999	1.1042 ± 0.0020	
−8419*	−6-c	5.5	A	1.0344 ± 0.0067	−272 ± 52	1995	1.1238 ± 0.0030	
−7470-1*	−8	7.5	ABA	1.0556 ± 0.0060	−435 ± 46	1986	1.2011 ± 0.0060	
−8420	−9-b	8.5	A	1.0064 ± 0.0064	−51 ± 51	1981	1.2677 ± 0.0074	
−8421	−10-a	9.5	A	0.9963 ± 0.0065	30 ± 52	1977	1.3363 ± 0.0088	
−8422	−11-b	10.5	A	0.9962 ± 0.0064	30 ± 51	1972	1.5143 ± 0.0191	
−7471-1*	−12	11.5	ABA	1.0148 ± 0.0057	−118 ± 45	1968	1.5943 ± 0.0100	
−8423	−13-c	12.5	A	0.9482 ± 0.0064	427 ± 55	1963	1.9387 ± 0.0782	
−8424	−14-a	13.5	A	0.9260 ± 0.0060	618 ± 52	1959	1.2210 ± 0.0031	
−9153	−14(ABA)	13.5	ABA	0.8823 ± 0.0080	1006 ± 73	1959		
−8425	−15-c	14.5	A	0.9120 ± 0.0060	740 ± 53	1954	0.9770 ± 0.0015	
−7472-1*	−16	15.5	ABA	0.9462 ± 0.0055	445 ± 46	1950	0.9800	445
−9150	−16(A)	15.5	A	0.8241 ± 0.0072	1554 ± 70	1950		
−9154	−16(ABA)	15.5	ABA	0.8599 ± 0.0075	1213 ± 70	1950		
−8448	−18	17.5	A	0.8877 ± 0.0091	957 ± 82	1940		
−9155	−18(ABA)	17.5	ABA	0.8372 ± 0.0074	1427 ± 71	1940		
−8480	−19	18.5	A	0.8760 ± 0.0091	1064 ± 84	1936		
−7473-1*	−20	19.5	ABA	0.9253 ± 0.0053	624 ± 46	1931	0.98	680
−9151	−20(A)	19.5	A	0.8414 ± 0.0078	1387 ± 75	1931		
−8481	−21	20.5	A	0.8874 ± 0.0092	959 ± 84	1923		
−8449	−22	21.5	A	0.8936 ± 0.0094	880 ± 84	1916		

(*Continued*)

Table 1. (*Continued*)

Lab code	Sample ID	Depth (cm)	Treat-ment	F_S	^{14}C age (yr BP)	#Year (CE)	F_{atm}	ΔT (years)
−9157	−22(ABA)	21.5	ABA	0.8416 ± 0.0080	1385 ± 76	1916		
−8482	−23-c	22.5	A	0.8886 ± 0.0093	949 ± 84	1908		
−7474-2*	−24-2	23.5	ABA	0.9324 ± 0.0072	562 ± 62	1900	0.98	640
−8450	−24	23.5	A	0.8662 ± 0.0090	1154 ± 84	1900		
−8483	−25	24.5	A	0.8760 ± 0.0094	1063 ± 86	1896		
−8451	−26	25.5	A	0.8814 ± 0.0095	1041 ± 86	1891		
−9158	−26(ABA)	25.5	ABA	0.7618 ± 0.0066	2186 ± 69	1891		
−8484	−28-c	27.5	A	0.8689 ± 0.0094	1129 ± 87	1882		
−7304*	−29	28.5	ABA	0.8931 ± 0.0091	908 ± 81	1878	0.98	980
−9152	−30(A)	29.5	A	0.6142 ± 0.0055	3915 ± 72	1873		
−9159	−30(ABA)	29.5	ABA	0.8607 ± 0.0076	1205 ± 71	1873		

Notes: Sample ID has a prefix of Shira GC4. Treatment A and ABA denote acid-treatment and acid-base-acid treatment, respectively. F_S is the fraction of modern carbon in samples calculated from measured $^{14}C/^{12}C$ ratios of OXII, sample and background, and corrected for $\delta^{13}C$ fractionation. When F_S is greater than 1, it means that the sample contains nuclear bomb carbon after AD1950. ^{14}C age = −8033×Ln(F_S) in 1σ error. #Year is determined from ^{137}Cs dating and comparison of Ca and Sr in Shira GC4 with historical lake level and salinity measurements. F_{atm} is the fraction of modern carbon of the atmospheric CO_2 determined by tree ring measurements (Hua et al. 2013). ΔT is the age difference between the measured ^{14}C age and the given #Year. * denotes the samples with minimum OCI and their ^{14}C ages are plotted in Figure 3b.

Seismic profiling of Lake Shira

Seismoacoustic equipment was employed (Krylov et al. 2019, 2022) for continuous seismic profiling of Lake Shira, enabling remote investigation of the lake bottom structure owing to the recording of acoustic waves reflected from the lake bottom. The seismoacoustic profiling was carried out using a purpose-built system, designed and manufactured on the base of Kazan Federal University (Krylov et al. 2015). The system includes a source of elastic waves, a receiver, a seismic station, a laptop, a GPS receiver, an inflatable boat, an electric motor, and power supply. The unit enables us to get seismic acoustic sections with vertical resolution of at least 15 cm; a depth study of various types of lake sediments of at least 10 m thickness; and a geodetic positioning system within several meters. It also provides the digital recording of information. An inductive oscillator "boomer" was used as a source of elastic waves. The seismic profile map of Lake Shira is shown in Figure 1D with the core location.

Results and discussion

^{210}Pb and ^{137}Cs profiles

The chronology of the sediment core is ascertained by measurements of the fallout radionuclides of ^{210}Pb and ^{137}Cs. Sediment accumulations of fallout ^{210}Pb and ^{137}Cs have been used extensively to date recent (<120 years) events in lacustrine environments. In the beginning, only odd-numbered samples (i.e., -1, -3, … etc.) were sent to the NTUAMS Lab for gamma counting. Thus, sample Shira GC4-1 is the sediment of 0–1 cm, and the depth of this sample is 0.5 cm (middle point of the one cm); and so on. The ^{210}Pb and ^{137}Cs curves are presented in Figure 2A and 2B respectively (See Supplement Table S1 for details). ^{210}Pb (half-life, $t_{1/2} = 22.3$ years) is a natural radioactive daughter of ^{222}Rn in the decay series of ^{238}U and is produced both in the atmosphere and the subsurface. The ^{210}Pb chronology for the studied samples has been obtained assuming a constant rate of supply model (Appleby and Oldfield 1992). Several assumptions must be taken before applying the ^{210}Pb age determination methodology: (1) constant amount of fallout ^{210}Pb, (2) ^{210}Pb deposition in sediment within a closed system, and (3) ^{210}Pb is immobile within sediment column (Saulnier-Talbot et al. 2009). The confidence in the ^{210}Pb dating method is enhanced with other proxies such as ^{137}Cs (an artificial and anthropogenic radionuclide). The ^{210}Pb activities of the studied samples show exponential decay of ^{210}Pb activity (Figure 2A). The total ^{210}Pb activity is much higher than that of ^{226}Ra, indicating the majority of ^{210}Pb comes from the atmosphere (excess ^{210}Pb). Even at the bottom of the core, the total ^{210}Pb is still greater than ^{226}Ra activity (Table S1), which means deficiency of ^{226}Ra (^{210}Pb and ^{226}Ra are not in secular equilibrium) in the lake sediments. The ^{226}Ra deficiency in the lake sediments might be caused by (1) the degassing of ^{222}Rn and (2) changes in ^{238}U and ^{226}Ra concentrations of the sediments due to the chemistry change of the lake. For instance, the ^{238}U and ^{226}Ra activities in the top 5 cm depth are very low (Table S1). In an anoxic environment, U forms U^{4+} ions which can be dissolved in water. The U concentration measured by ICPOES supports this scenario (Figure S5a). In such a circumstance, the supported ^{210}Pb cannot be determined by ^{226}Ra (or (^{214}Pb+^{214}Bi)/2).

In Figure 2A, the total ^{210}Pb below 19 cm depth is relatively constant, so one can use the total ^{210}Pb activity at this depth as the supported ^{210}Pb activity. Using the total ^{210}Pb activity in each layer above this depth subtracting this supported ^{210}Pb activity, one can obtain an excess ^{210}Pb profile. The exponential fitting of the excess ^{210}Pb profile provides the average sedimentation rate which equals –0.0311/slope of the fitting. Based on the ^{210}Pb dating and constant rate of supply model (Appleby and Oldfield 1992), the average linear sedimentation rate of the upper 19 cm part is 0.229 cm/yr.

The peak of the nuclear bomb produced ^{137}Cs profile shown in Figure 2B indicates that the 12.5 cm (12–13 cm) depth should have an age of 1963 CE. Based on the coring year (2020 CE), one can estimate the linear sedimentation rate in the upper 13 cm part, to be 0.22 cm/yr (Figure 2B). This linear sedimentation rate is very close to the estimate (0.229 cm/yr) from the ^{210}Pb profile, indicating both dating results are reliable. Previous studies have found that ^{137}Cs peaks in lake sediments and peat
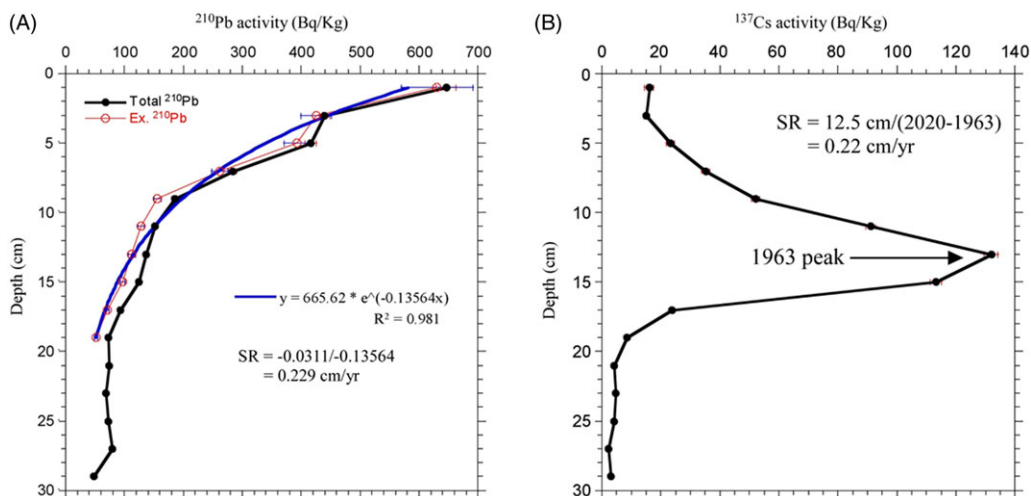
Figure 2. (A) the natural fallout radionuclide ^{210}Pb profile; (B) artificial fallout radionuclide ^{137}Cs profiles in Lake Shira GC4 core samples.

profiles may experience a post-depositional downward shift (Baskaran et al. 2017; Le Roux and Marshall 2010/2011; Li et al. 2019; Misra et al. 2024; Rowan et al. 1992) owing to the increased solubility of ^{137}Cs by percolating water and changing pH. However, this situation does not appear to be the case in saline Lake Shira. Kalugin et al. (2013) also found the ^{137}Cs peak (indicating 1963 CE) at 9.2 cm depth in the sediments of a box core Shira 2010. In the present study, Shira GC4 core was collected in 2020 i.e. around 10 years later than Shira 2010. The ten years of deposition would add 5 cm of sediments, which would result in the ^{137}Cs peak representing 1963 CE at 13 cm depth in the Shira GC4 core. This consistency further supports the reliability of our ^{137}Cs chronology.

AMS ^{14}C dating and OCI

The 35 AMS ^{14}C dates of the Lake Shira GC4 core are presented in Table 1. The AMS dating was performed on the pre-treated (acid and acid-base-acid) bulk sediments of the core owing to the lack of plant remains. The samples above 12 cm depth show a fraction of modern carbon ^{14}C (F_S) >1 (Table 1), reflecting the presence of bomb carbon and a deposition age after 1950 CE. However, the ^{14}C activity is much lower than the atmospheric CO_2 at that time (the highest F_{atm} in 1963 was 1.9387) (Figure S2) (Hua et al. 2013), implying an old carbon influence (OCI) exists in the ^{14}C ages. Since TOC in the lake sediment is not mobile (Misra et al. 2024), the nuclear bomb ^{14}C curve in the core illustrates that the upper 12 cm part was deposited after 1950 CE. Although Figure 3b shows that the highest ^{14}C activity at the 7 cm depth of the studied core which may reflect the 1963 ^{14}C peak is the nuclear bomb ^{14}C curve, this depth is shallower than the 1963-peak depth determined by the ^{137}Cs profile (Figure 3a). Since the ^{14}C activity of lake sediments can be strongly affected by the OCI evidenced by much lower than the atmospheric $^{14}CO_2$ (Figure S2), the ^{14}C peak at 7-cm depth cannot be used for the 1963 peak. In Figure 3b and Figure S2, the ^{14}C ages below 16-cm depth are older than 445 yr BP, much older than the ^{137}Cs dating chronology. Since the chronology below 19-cm depth may be beyond 120 years, using ^{210}Pb and ^{137}Cs methods is uncertain (Figure 3a). Shira GC4 core was subsampled in the field, so that varve counting cannot be performed in this case. Furthermore, the white carbonate zone from 16 to 23 cm depths does not contain clear laminations for counting, so from this depth on the core is not amenable to varve counting. Therefore, the first task is to establish a reliable chronology of the Shira GC4 core to assess the OCI in the ^{14}C ages and their causes. This information is used to suggest the best way to build up a reliable chronology for sediments older than 200 years.
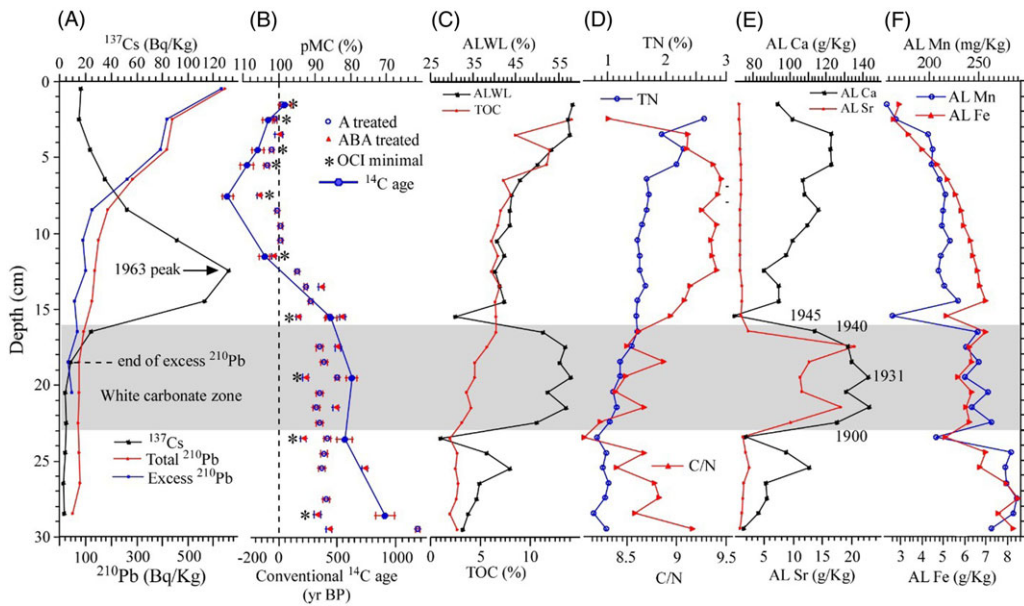
Figure 3. *Comparisons of ^{14}C dating results with ^{210}Pb and ^{137}Cs as well as selected elemental profiles. (A) ^{210}Pb and ^{137}Cs profiles. (B) ^{14}C results. The triangle denotes the ^{14}C measurements of ABA-treated samples, whereas the square symbol denotes the ^{14}C measurements of A-treated samples. The blue curve is the conventional ^{14}C age calculated by the selected less OCI samples (noted with an asterisk *) marker. The vertical dashed line indicates modern ^{14}C. Points on the left side of this line contain nuclear bomb ^{14}C which should be post 1950 CE. (C) ALWL (0.5N HCl leach weight loss) and TOC. (D) TN and C/N. (E) AL Ca and Sr (salinity indicator). (F) AL Mn and Fe (Redox condition proxy).*

Chronology of Shira GC4

As mentioned before, the chronology between 0 and 13 cm can be determined by the ^{137}Cs peak at 12–13 cm, assuming that the linear sedimentation rate of 12.5 cm/(2020–1963) remains constant. Below the 13 cm depth of Shira GC4, there is a zone containing high ALWL (acid leach weight loss) values, AL Ca and Sr correspond to carbonate zones in many gravity cores from Lake Shira (Dar'in et al. 2015; Kalugin et al. 2013; Rogozin et al. 2010, 2020; Zykov et al. 2012) (Figures 3c, 3e and Figure S3). Right above this white carbonate zone, Rogozin et al. (2020) and Zykov et al. (2012) showed a rapid increase in okenone which reflects anoxic conditions in Lake Shira around 1945 (Figures S3b, S3c and S3d). In Figure 3f, a strong drop in AL Mn and Fe corresponded to anoxic conditions. Therefore, 1945 CE is assigned to 15.5 cm depth. The comparison of ALWL, AL Ca and Sr contents with measured lake level and salinity allows us to determine the chronology between 16 cm and 24 cm. The high values of ALWL, AL Ca and Sr in Shira GC4 represent high salinity and low lake levels during 1940–1900 (Kalacheva et al. 2002; Rogozin et al. 2010). Hence, we assign the ages of 1940 CE and 1900 CE for 17.5 cm and 23.5 cm depths in Shira GC4, respectively (Figure 3e). According to Zykov et al. (2012) and Rogozin et al. (2020), the lowest measured lake level (highest salinity) was in 1931. Thus, 1931 CE is assigned to 19.5 cm depth. With these known ages at these depths, one can calculate ages between 13 cm and 24 cm depths of Shira GC4. Below 24 cm depth, there is no solid evidence to support an absolute chronology. We use the sedimentation rate between 12.5 cm (1963 CE) and 16.5 cm (1945 CE) to apply to 24–30 cm depth, as the lamination patterns in the two zones are similar. Following such a construction, the age at the bottom (30 cm) of Shira GC4 is 1870 CE (equivalent to a calibrated ^{14}C age of 80 cal yr BP). On the other hand, the measured ^{14}C age at the end of the core is about 890 cal yr BP, showing a large old carbon influence (OCI). In the next section, we will discuss the cause and variation of the OCI.

Cause and estimation of OCI on the ^{14}C age of the core

For ^{14}C dating of lake sediments, it is essential to understand the complicated carbon sources and conduct the various treatments to eliminate contamination and OCI. The role of old carbon recycling in the sediment plays a significant role in imparting the "radiocarbon reservoir effect" (Ojala et al. 2019). The OCI or "radiocarbon reservoir effect" of Lake Shira were previously documented by many researchers. Kalugin et al. (2013) and Dar'in et al. (2015) used ^{137}Cs dating, varve counting and Ca/Sr measured by XRF to determine the sedimentation rate of ∼0.2 cm/yr in the upper 10 cm sediments in Lake Shira. This sedimentation rate is close to the results of our ^{137}Cs and ^{210}Pb dating in Shire GC4 (Figure 2). However, the chronology below 10 cm depth has utilized TOC ^{14}C dates from the sediments and varve counting at various depths in Kalugin et al. (2013). Furthermore, ^{14}C dating was achieved by subtracting a ^{14}C age of 1275 years (Dar'in et al. 2015) or 1200 years (Kalugin et al. 2013), to account for the radiocarbon reservoir effect (Wilkins et al. 2012). The previous studies attributed the old carbon influence (OCI) in the overall ^{14}C age to the carbonate radiocarbon reservoir effect as Lake Shira is a saline lake. In this study, our ^{14}C ages were dated on organic carbon, so that no direct influence from inorganic carbon (carbonates). It is necessary to find out how the OCI exits in ^{14}C ages of organic carbon (TOC) in Lake Shira sediments.

Figures S2 and 3 illustrate the OCI in the ^{14}C dating of total organic carbon (TOC) in Shira GC4. In Figure 3b, although the ^{14}C ages in the upper 12 cm contain nuclear bomb ^{14}C, indicating deposition after 1950 CE, their ^{14}C activities are much lower than that of the contemporary atmosphere due to the OCI. At 15.5 cm depth, the correct depositional age is 1950 CE, but the measured ^{14}C age is 445±46 yr BP (Table 1 and Figure S2). In Table 1, ∆T exhibits OCI variations at different layers (time) selected for minimal OCI ages. This study demonstrates that: (1) OCI exists in the ^{14}C age of TOC; (2) the OCI varies with time; (3) ABA treatment does not remove the OCI; (4) the OCI can be as small as 100 years or less. Therefore, if OCI was small, the ^{14}C dating on those samples may still be reliable. The estimation of OCI and its implications are discussed below, based on our dating results.

Significant uncertainties persist in ^{14}C dating on account of the differential radiocarbon reservoir effect on various dating materials (Jiang et al. 2022). Generally, plant materials are regarded as the most suitable materials for ^{14}C dating owing to the absence of any radiocarbon reservoir effect (Hattė et al. 2001). However, no plant macrofossils exist on the Shira GC4 sediment core. All samples for ^{14}C dating in this present study are pre-treated bulk sediments. In addition, the samples were pre-treated either with acid (A) or acid-base-acid (ABA) methods, so that there was no direct influence of carbonates in the sediments. Despite thorough pre-treatment, OCI is still present in the ^{14}C dating. Therefore, we distinguish between OCI on TOC ^{14}C ages and the hard water "radiocarbon reservoir effect" which accounts for old carbon from inorganic carbon sources and aged HCO_3- and CO_3^{2-} in water bodies. In general, TOC in lake sediments contains organic carbon from (1) organic carbon formed in equilibrium with atmospheric $^{14}CO_2$ ($[^{14}C/^{12}C]_{atm}$); (2) aquatic submerged plants and algae that may have incorporated aged carbon through photosynthesis ($[^{14}C/^{12}C]_{MOC}$) by dissolved CO_2 in water; (3) reworked organic carbon from soils carried by surface runoff ($[^{14}C/^{12}C]_{ROC}$); and (4) organic carbon formed by the photosynthesis of anoxic bacteria at the lake bottom ($[^{14}C/^{12}C]_{POC}$), e.g., pigments such as carotenoids (Rogozin et al. 2010, 2020; Zykov et al. 2012). The mass balance equation for the ^{14}C distribution of TOC in the lake sediments is:

$$\left[^{14}C/^{12}C\right]_S = f_1 \times \left[^{14}C/^{12}C\right]_{atm} + f_2 \times \left[^{14}C/^{12}C\right]_{MOC} + f_3 \times \left[^{14}C/^{12}C\right]_{ROC} + f_4 \times \left[^{14}C/^{12}C\right]_{POC}$$

$$(1)$$

$$f_1 + f_2 + f_3 + f_4 = 1 \tag{2}$$

By dividing Equation (1) by the $^{14}C/^{12}C$ of modern ^{14}C at 1950 ($[^{14}C/^{12}C]_{std.1950,}$), Eqn. (1) can be re-written as:

$$F_S = f_1 \times F_{atm} + f_2 \times F_{MOC} + f_3 \times F_{ROC} + f_4 \times F_{POC} \tag{3}$$

In Equation (3), F_{atm} stands for the ^{14}C activity in atmospheric CO_2. This value is assumed to be in the range between 0.98–0.99 before 1950 CE (Hua et al. 2004; Stuiver et al. 1998). After 1950 CE, due to the nuclear bomb ^{14}C influence, F_{atm} reached a maximum of 1.93 in 1963–1964 CE (Table 1) (Hua et al. 2013). F_{atm} decreased to 1 around 2020 CE (Hua et al. 2022; Reimer and Reimer 2024) due to fossil CO_2 emissions and nuclear bomb ^{14}C decay. Most plants grown in the atmosphere should have F_{atm} values that provide the true age of organic carbon. However, the term F_{POC} often contains OCI, especially in a meromictic lake. For example, Rogozin et al. (2020) found that organic carbon components such as okenone at the bottom of the lake used the photosynthesis of anoxic bacteria that eventually utilized old, dissolved CO_2 from the saline lake. Hence, F_{POC} may be expected to contain significant OCI. The fraction of F_{POC}, f_4, varies with lake stratification and redox conditions. The variable okenone concentrations are also evident in Lake Shira sediments (Rogozin et al. 2020; Figure S3), where okenone peaks signify lake transgressions and the absence of okenones denote periods of stable or decreasing water level. During a holomictic lake stage, dissolved CO_2 in the lake water can exchange with atmospheric CO_2 and hence OCI will decrease. In contrast, a maximum OCI level is apparent during a meromictic lake stage owing to the non-exchange of atmospheric CO_2 in different water layers.

Reworked organic carbon from surface runoff (F_{ROC}), can contain OCI as well. In general, terrestrial plants reflect only F_{atm}. However, if the organic carbon in soil was aged before it was brought into the lake, then the OCI would exist. Surface runoff is the prime transport mechanism for this carbon. For example, when mountain glaciers melt, the melting glacier could not only erode land surface, but also release trapped CO_2, both bringing old carbon into the lake. One situation may be caused by human activity. For instance, human fertilizer may contain old carbon. Or, human development that disturbs natural land surfaces to create new farmland. Such activities would bring old carbon with F_{ROC} into a lake. Lake Shira is located in a remote area with minimal human activity. Thus, reworked TOC in Shira GC4 is mainly due to surface runoff which is related to climate. The value of f_3 should be greater with increased lake level caused by increased surface runoff. But, if F_{ROC} is closed to F_{atm} during deposition, this term should not affect OCI.

The term F_{MOC} denotes the organic carbon from aquatic submerged plants and algae living in the mixolimnion zone of a lake (Figure S1). Many previous studies have found that aquatic submerged plants and algae use dissolved CO_2 for photosynthesis (e.g., Chen et al. 2021 and references therein). If the water body has an equilibrium of ^{14}C activity between aquatic dissolved CO_2 and atmospheric CO_2, then this term would not contain OCI. However, for Lake Shira, the ^{14}C activity of the dissolved CO_2 in lake water can be much lower than that of atmospheric CO_2, because of four reasons: (1) high CO_2 input from groundwater which brings dead carbon; (2) weak CO_2 exchange with the atmosphere due to strong lake stratification during the meromictic stage; (3) no CO_2 exchange with atmospheric CO_2 when the lake surface is covered by ice (currently 7 months per year); and (4) old glacial meltwater into the lake. Hence, when the lake is at a fresh, holomictic and high productivity stage, f_2 is greater and F_{MOC} is closer to F_{atm}. The OCI at this stage is minimal; and vice versa.

Currently, f_2, f_3, f_4, F_{MOC}, F_{ROC} and F_{POC} in Eqn. 3 are unknown. In order to estimate these terms, a detailed study of ^{14}C dating on samples of lake water, groundwater, aquatic plants, algae, sediment trap particles and surrounding soil should be carried out. Nevertheless, these terms vary with the lake conditions under different climates. Therefore, the OCI on the ^{14}C age of TOC in Lake Shira sediments is not constant. Both A and ABA treatments may not be able to remove OCI completely.

Figure S3 illustrates the carbon sources and the pre-treatments to deal with different components in the lake sediments. Both A and ABA treatments can remove carbonates, so that no direct influence of carbonates on the ^{14}C ages. ABA treatment can further eliminate humic acid (HA; Misra et al. 2024).

1. The conventional ^{14}C age curve shown in Figure 3b is used for the ages with the least OCI. Those ages are mainly ABA-treated samples below 5.5 cm depth, except one age at 19.5 cm depth. This means that the ABA treatment can remove more OCI.

2. There are eight samples which have both A and ABA-treated ^{14}C ages (Table 1). In these 8 pairs of ^{14}C ages, samples from 15.5, 19.5 and 23.5 cm depths have younger ABA-treated ^{14}C age than A-treated ^{14}C age, and samples from 13.5, 17.5, 21.5, 25.5 and 29.5 cm depths have the opposite scenario. This phenomenon may be explained by the TOC formed under different lake conditions. As the geochemical data will be shown later (next section), Lake Shira had low surface runoff, low lake level and low productivity but relatively high salinity at 15.5, 19.5 and 23.5 cm depths, reflected by low ALWL and major elements especially in AR phase (Figure 4), and low TOC (Figure 4g). The majority of the TOC at those depths would be produced in lake water with less reworked TOC from surface runoff, so that the OCI from $f_3 \times F_{ROC}$ was small. However, the TOC from aquatic submerged plants and algae may use dissolved CO_2 in the saline lake water which contains old carbon. This part of TOC can form humic acids (HA) which are not eliminated with A treatment, but can be removed by ABA treatment (Misra et al. 2024). On the other hand, the organic carbon produced by the photosynthesis of anoxic bacteria at the bottom lake ($f_4 \times F_{POC}$) should be minimal at depths of 19.5 and 23.5 cm because of holomictic conditions (Rogozin et al. 2010, 2020; Zykov et al. 2012). Although the highest okenone content at 15.5 cm was 3000 µg/g TOC (= 0.3% of TOC) (Figure S3c), its fraction was quite small compared to 5% TOC in the sediments. Consequently, the ABA-treated ^{14}C ages at these depths have the least OCI.

3. The samples at 13.5, 17.5, 21.5 and 25.5 cm depths have younger A-treated ^{14}C age than ABA-treated ^{14}C age in the paired ages. This situation may be explained by the removal of the humic acids (HA) with higher ^{14}C activity than that of the Humin (HM) by ABA treatment (Misra et al. 2024) and F_{POC}. In Shira GC4, the highest salinity appeared in the white carbonate zone between 17 and 23 cm depths. Four A-treated ^{14}C ages ranged from 880 yr BP to 959 yr BP (Table 1), which may reflect the "radiocarbon reservoir effect" of OCI by uptake of dissolved CO_2 owing to the absence of Carotenoid formation in holomictic lake condition. Furthermore, four A-treated ^{14}C ages show relatively high nuclear bomb ^{14}C signal and 3 A-treated ^{14}C ages show weak nuclear bomb ^{14}C signal, indicating that the OCI caused by the uptake of dissolved CO_2 in the lake water for photosynthesis of aquatic submerged plants and algae did not access nuclear bomb ^{14}C signal. With changing salinity and lake productivity, the term of $f_2 \times F_{MOC}$ varies, being lower salinity and higher lake productivity, the less OCI. The increasing A treated ^{14}C age from "modern" above 8.5 cm depth to 618±52 yr BP at 13.5 cm depth demonstrates that the OCI from "radiocarbon reservoir age" of Lake Shira on TOC ^{14}C age should be less than 700 years since 1963 CE.

4. The OCI from humin (HM) and pigment in the TOC of the lake sediments due to the utilization of dissolved CO_2 in the bottom water during meromictic lake conditions are difficult to remove with the ABA treatment. However, the meromictic condition can be detected by carotenoid measurement and redox-sensitive elements such as Mo/Mn, etc. For example, the carotenoid content below the white carbonate zone was very low (Figure S3), so the term of $f_4 \times F_{POC}$ could be very small in the ancient lake.

In summary, old carbon influence (OCI) is not constant. It varies with the physical and chemical conditions of the lake under different climate regimes. ^{14}C dating of the lake sediments requires ABA treatment. The best way for the construction of a reliable age-depth model for a sediment core >200 years is a multi-proxy approach by combining high-resolution ^{14}C dating with geochemical analyses. The periods of low salinity, low surface runoff and high productivity lake conditions have the least "radiocarbon reservoir effect."

Geochemical and magnetic records

Geochemical characteristics of lake sediments can provide information on provenance, weathering, sedimentation processes, salinity, temperature and hydrological conditions (Wittkop et al. 2020; Yang
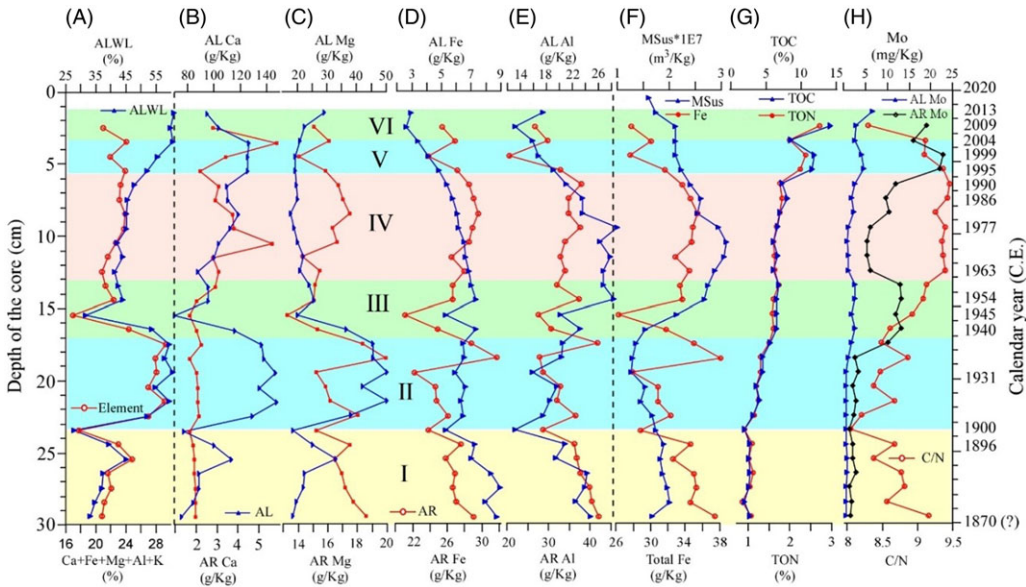
Figure 4. *Geochemical indices and magnetic susceptibility in the Lake Shira GC4 core in seven zones. AL = acid-leachable; AR = Aqua Regia dissolution; TD denotes total concentration, = AL + AR. ALWL = acid leach weight loss. Note that the concentration units are different for different elements.*

et al. 2021). Therefore, the geochemical and elemental records of Lake Shira (Figure 4 and Figure S5) provide valuable insight into lake history and past climate influence (Skurzyński et al. 2020; Zhao et al. 2019).

Total organic carbon (TOC), total organic nitrogen (TON) and C/N ratios of the studied samples

In order to identify organic matter sources in sediments, it is possible to use the ratio between carbon and nitrogen as an indicator, i.e. the C/N ratio (Kaushal and Binford, 1999; Gälman et al. 2008; Kaushal and Meyers 2003; Perdue and Koprivnjak 2007; Routh et al. 2004). Figures 4g and 4h show the variations of TOC%, TON% and C/N. First of all, the TOC% and TON% are strongly positively correlated ($R^2 = 0.991$), indicating a common source for C and N. As mentioned earlier, we did not find any plant remains or animal shells in the core. The organic matter (OM) was low (TOC < 3%) before 1900 CE (below 24 cm depth), then gradually increased to 6.5% around 1940 CE (at 17 cm depth), and remained relatively constant until 1990 CE (at 7 cm depth). After 1990 CE, TOC strongly increased from 6.5% to 14.2%. The OM variation reflects lake productivity and redox conditions. Higher TOC% indicates higher productivity and a more reducing environment. In general, soil TOC% is low compared to lake sediments. Hence, higher terrestrial input would reduce OM% in the lake sediments. Therefore, the observed OM trend shows that relatively high terrestrial input (surface runoff) resulted from wet climatic conditions before 1900 CE. The lake was fresh with relatively low productivity and moderate oxidation. Increased OM% during 1900~1940 CE might have resulted from (1) a drop in the lake level due to evaporation which led to an increase in nutrient concentration, (2) reduced surface runoff and (3) increased lake productivity due to enhanced water temperature and nutrient concentration. As discussed earlier, the 17–23 cm layer in Shira GC4 corresponded to a "white carbonate" zone between 13 and 18 cm depths in previous cores. This "white carbonate" zone was considered a cold period of lake level drop, which in turn supported an OM increasing trend due to enhanced nutrient concentrations. The relatively constant OM% during 1940–1990 CE (17–7 cm depth) implies that the lake sediments had little change.

A C/N ratio in lakes between 4 and 10 is typical for OM that originates from non-vascular (algal) production (Meyers and Ishiwatari 1993), while the C/N ratio of approximately 20 indicates terrestrial vascular plant input (Meyers 1997; Schubert and Calvert 2001). The C/N ratio of the studied sample ranging from 8 to 9.5 (Figure 4h) is consistent with the mainly algal input of lacustrine sediments. However, we may use C/N values to illustrate the ratio of exogenous and endogenous OM, as higher C/N ratios imply higher exogenous/endogenous OM ratios. Figure 4h shows that C/N fluctuated between 8.07 and 9.45, with a maximum at around 1990 CE and a minimum of around 1900 CE, suggesting that the exogenous/endogenous OM ratio changed with lake productivity and surface runoff. A general C/N decreasing trend from 1870 CE to 1900 CE (30–24 cm) indicates a reduced exogenous OM source owing to decreased surface runoff under a relatively dry climate. The fluctuating but increasing trend of C/N from 1900 CE to 1940 CE implies that the endogenous OM (lake productivity) budget was controlled by vertical water mixing that affects nutrient concentrations and light penetration in the lake. Continuously increasing C/N values from 1940 CE to 1963 CE indicate enhanced exogenous OM in the lake sediments. However, the majority of the OM was still associated with lake productivity, as the lake was strongly stratified, anoxic and meromictic. The C/N during 1963~1995 CE remained stable and elevated, probably reflecting high exogenous OM because of terrestrial input under human activity. The decreasing trend in C/N since 1995 CE implies strongly increased endogenous OM with high lake productivity involving human impact.

Elemental concentrations from HCl leachate and Aqua Regia dissolution

Elemental concentrations measured by ICPOES contain two fractions: 0.5N HCl acid-leached elements (AL) and Aqua Regia microwave-digested elements (AR) (Figures 4 and S5). The AL elements are influenced by lake water geochemistry and the AR elements reflect lake sediment characteristics. Because the samples for AR analysis were residues of the AL analysis, the total elemental concentration (TD) of an element equals its AL concentration plus AR concentration. These are presented in Figures 4 and S5, with some elemental concentrations in g/kg and others in mg/kg.

Figure 4a exhibits changes in the acid leach weight loss (ALWL%) and total Ca, Fe, Mg, Al and K concentrations, showing strong covariance except for the top 6 cm of the core. All five elements are concentrated in AL fraction. We shall start with them first. As mentioned earlier, 0.5N HCl acid leach should not attack the detrital phase and organic phase. Hence, AL elements mainly come from acid-soluble minerals such as carbonates, absorbed particles on the sediment surface and those dissolved in porewater. For this reason, Ca, Mg and Sr are dominant in the AL phase (Figures 4a, 4c and S5b). As those three elements prefer to co-precipitate with carbonate which favours high alkalinity and salinity. Hence, the higher AL Ca, Mg and Sr concentrations represent higher lake water alkalinity and salinity. This is clear in the AL Ca, Mg and Sr concentrations during 1900~1940 CE (24–17 cm). This high AL Ca, Mg and Sr concentration zone corresponds to the "white carbonate" layer around 13–18 cm in the previous Shira cores (Figures 3, 4 and S5) discussed earlier. Although the "white carbonate" layer confirms our elemental results, the OM trends differ between the previous studies and Shira GC4. The OM of the previous cores were measured by Loss on Ignition (LOI) at 550ºC, whereas TOC (%) was determined by CO_2 liberated at 950ºC in an Elemental Analyzer (EA); and is considered as absolute organic carbon content (Rogozin et al. 2016a) (Figure S7). The OM measured by LOI of the Shira 2016 core was lower than before and after the "white carbonate" zone, but TOC increased in the carbonate zone in Shira GC4 (Figure S7). The increasing trend of TOC can be explained by elevated lake productivity owing to the lake shrinking in the early stage and well-mixed water column (holomictic) in the later stage of the white zone.

Nevertheless, we can use the AL mineral concentrations in Shira GC4 to illustrate lake chemistry changes. Based on their variations (Figures 3, 4, S3, S5, S7), we can classify six zones: Zone I (1870–1900 CE, 30–24 cm), whose concentrations increased from low to moderately high, reflecting fresh lake water. At the end of this zone (ca. 1900 CE), we observe minimal AL mineral concentrations. In Zone II

(1900–1940 CE, 24–17 cm), these AL mineral concentrations peaked, reflecting a cold, saline and holomictic lake stage (Kalugin et al. 2013; Rogozin et al. 2020; Zykov et al. 2012). In Zone III (1940–1963 CE, 17–13 cm), AL Ca, Mg and Sr concentrations dropped significantly in the early interval (from 17 cm to 15 cm depth), then Ca, Mg and Sr behaved differently: AL Sr and Mg remained low continuously in the upper 15 cm part, but AL Ca increased from 15 cm to 7 cm depth (from 1950 CE to 1986 CE). In Zone IV (1963–1994 CE, 13–7 cm), the lake increased in salinity, as shown by increased AL Ca and in lake productivity with enhanced TOC and TON, except at the end of this stage (7–6 cm, 1990 CE). In Zone V (1994–2003 CE, 6–4 cm), high AL Ca, TOC and TON reflect high salinity and lake productivity. In Zone VI (2003–2020 CE, 4–0 cm), AL Ca dropped significantly, but TOC and TON increased. The opposite trends of organic carbon (TOC) and inorganic carbon (AL Ca) with a drop in C/N ratio probably imply that Lake Shira became a stratified and anoxic lake, and even meromictic for some years, which is supported by the high okenone contents from 1995 to 2013 in the Shira 2013, 2016 and 2017 cores (Figure S3) (Rogozin et al. 2020).

Fe, Mg, Al, K and Ti are all considered lithophilic and terrigenous elements and their variations are predominantly controlled by detrital input (Dobrovolsky 1999). Their concentrations are normally dominated in the AR (detrital) fraction (e.g., Figures 4d and 4e). AR Fe, Mg and Al trends show similar patterns, implying they are all generated from the detrital phase. In addition, Fe and Al can be leached out as oxides (FeO, Fe_2O_3, Fe_3O_4, Al_2O_3, etc.) that exist in terrigenous material. Thus, the AL Fe and Al generally follow the AR Fe and Al trends (Figures 4d and 4e). There are two exceptional periods in the records: 1936~1940 CE (19–17 cm) and after 1963 CE. During 1936~1940 CE, the AL Fe and Al did not follow the AR Fe and Al fluctuations. This interval was the latter part of the "white carbonate zone." Although the cause of such a disparity is unclear, we suspect that the significant OM formation may play an important role. An increase in OM content will enhance the consumption of oxygen in the lake and lead to a reducing condition. Fe and Al are preferentially dissolved in lake water under a reduced environment and preferentially precipitated as oxides in the lake sediments when the lake has an oxide condition. A positive correlation between AL Fe and AL Mn ($R^2 = 0.679$; Figure 3f) supports this interpretation as both Fe and Mn similarly correspond to redox conditions.

Thus, terrigenous input of the lake is reflected by AR Fe, Mg and Al, whereas AL Fe and Al may help us in understanding lake chemistry change. The AR Fe, Mg and Al exhibit a generally decreasing trend from 1870 CE to 1900 CE, reflecting decreasing surface runoff. A strong rebound of terrigenous input occurred during 1931~1936 CE as shown by elevated AR Fe, Mg and Al, then a decline of terrigenous input from 1936 to 1945 CE; as seen in the decreasing trends in AR Fe, Mg and Al (Figures 4c, 4d and 4e). Changes in terrigenous input indicated by AR Fe, Mg and Al should be controlled by surface runoff. In Figure S6, the measured lake level increased from 1930 to 1940 and level out during 1945~1955. This supports the interpretation of the AR Fe, Mg and Al variations in the white zone. The general decreasing trends of AL Fe and Al with increasing TOC and TON trends from 14 cm (prior to 1964 CE) to 2 cm (2011 CE) reflect enhanced reducing conditions (Figures 4d, 4e and 4g).

Molybdenum (Mo) is a redox-sensitive trace element. Mo was used in chemical fertilizers in the early 20th century but was banned from use after the 1970s. Therefore, human impact may be reflected by the Mo abundance in marine and lake sediments. Authigenic Mo precipitation only proceeds in the presence of free dissolved HS^- in water under a reducing environment (Crusius et al. 1996). In Figure 4h, Mo is seen mainly in the AR fraction, but AL Mo and AR Mo are strongly correlated ($R^2 = 0.946$). The TOC % is also correlated with AL Mo and AR Mo concentrations, with a slightly higher correlation coefficient with AL Mo ($R^2 = 0.842$) than AR Mo ($R^2 = 0.739$). Thus, one can use both AL and AR Mo as an indicator of redox conditions. Figure 4h shows that both AL and AR Mo concentrations were very low before 1936 CE, indicating a relatively oxidizing environment. The elevated AL and AR Mo concentrations during 1936~1940 CE (19–17 cm) indicate that the environment became more reducing. Relatively high AL and AR Mo concentrations during 1940~1963 CE (17–13 cm) illustrate that the lake environment was strongly reducing condition (Figure 4h). Zykov et al. (2012) and Rogozin et al. (2020) reported high biogenic pigment contents in this interval, which support our finding of strong reducing conditions. After 1963 CE, both AL and AR Mo concentrations dropped to relatively low

concentrations between 1963 and 1977, then increased until 1994 CE. The highest AR Mo contents appeared between 1994 and 2003 when the biogenic pigment also peaked (Rogozin et al. 2020).

Manganese (Mn) is a well-known redox-sensitive element. It normally precipitates in an oxidizing environment as MnO_2 but dissolves in water under reducing conditions. AR Mn represents terrigenous input with surface runoff, whereas AL Mn (authigenic fraction, i.e., particle formation in the lake water) reflects Mn precipitation in the lake water. Figure S5c shows the variations of AL Mn and AR Mn in the core. The AL Mn had a generally decreasing trend from the bottom (older time) toward the top (the present) except for two periods (around 1900 CE and 1945 CE) when surface runoff became low. The long-term decreasing trend of AL Mn reflects a change from oxidizing conditions to reducing conditions. This trend agrees with the interpretations and AL Fe, AL Al, AR Mo and the TOC and TON trends. AL Mn is positively correlated with AL Fe ($R^2 = 0.679$) (Figure 3f), but AR Fe and AR Mn are not correlated. The correlation between AL Fe and AL Mn provides a further indication of changing redox conditions in the lake. The opposite trends observed for AL and AR Mn during 1936~1940 CE (the later part of Zone II) are also observed in AL and AR Fe and Al (Figure 4d and 4e), perhaps due to significant organic matter formation in the lake. Moreover, as both Mo and Mn are sensitive to redox conditions, total (TD) Mo/Mn in the sediments may be a better indicator of redox conditions, with higher Mo/Mn reflecting more anoxic conditions. In Figures S6 and S7, the comparison among the lake level, TD Mo/Mn and okenone-rich layers illustrate this sensitivity.

Cu, Zn and Pb are trace metal elements. Their abundance in natural sediments is very low. Figures S5d, S5e and S5f reveal Cu, Zn and Pb variations in Shira GC4. The AR fraction of Cu and Zn is a dominant phase, whereas the AL fraction of Pb was dominant before 1998 CE but reversed after 2000 CE (Figure S5f). AR fractions reflect terrigenous input, while AL fractions are functions of organic content and pH, salinity and lake water temperature. AR Cu, Zn and Pb concentrations in the sediments sharply increased after 2000 CE, indicating an industrial (human) influence. Cu, Zn and Pb can be bound by organic matter which may not be released by a 0.5N HCl leach, but may be dissolved by Aqua Regia microwave digestion. The source of AL Cu, Zn and Pb comes from both surface runoff and atmospheric fallout. Before 1959 CE (14 cm depth), the AL Cu, Zn and Pb concentrations were chiefly affected by surface runoff and OM formation. Relatively high AL concentrations in Zone I are accompanied by low OM formation and high surface runoff. The decline of AL Cu, Zn and Pb concentrations in the earlier half of Zone II was due to reduced surface runoff. After 1936 CE, AL Cu, Zn and Pb increased with enhanced OM, reducing conditions and surface runoff until 1945 CE. High and increased AL Cu, Zn and Pb during 1950~1995 are attributed to OM and anthropogenic input. The decreasing trends in AL Cu, Zn and Pb concentrations since 1994 CE can be explained by organic matter influence as increased OM can absorb more Cu, Zn and Pb so that their concentrations in the AL phase would be lower. On the other hand, the AR Cu, Zn and Pb would not be affected by OM. The strong increase in AR Cu, Zn and Pb in Zone VI is likely due to terrestrial input affected by human activity.

In summary, elemental concentrations in lake sediments should be separated into 0.5N HCl AL and AR phases. The AL fraction reflects mainly the influence of lake chemical conditions, whereas the AR fraction represents more terrigenous input with surface runoff and atmospheric fallout. AL Ca, Sr and Mg are indicators of lake salinity, alkalinity and pH. AL Mo, Mn, Fe, and Al are indicators of the redox condition of the lake. TOC%, TON% and C/N are proxies for lake productivity. Cu, Zn and Pb concentrations may be used for detecting human impact.

Magnetic record

The measured magnetic bulk susceptibility (MSus) values of Shira GC4 vary from $(1.285~2.973) \times 10^{-7}$ m^3/kg (Figure 4f). In this study, we attempt to understand how MSus of lake sediments respond to climate and environmental change. First of all, MSus mainly comes from iron minerals such as magnetite (Fe_3O_4) and hematite (Fe_2O_3). Therefore, a comparison of MSus and total Fe concentration

(AL + AR) is shown in Figure 4f. The comparison generally agrees with the positive relationship except during the period of 1936~1940 CE (later part of the white carbonate zone) when total Fe was high but MSus was low. Rogozin et al. (2020) attributed the low magnetic signal in this "white carbonate" zone to low biogenic magnetite under holomictic and oxidizing conditions. On the other hand, as discussed before AR Fe is the majority of total Fe and reflects terrestrial input. The elevated total Fe during 1936~40 CE represented lake level rebound due to the enhanced surface runoff, but biogenic magnetite could not form until the lake became anoxic. Another proxy comparable to the MSus profile is the C/N profile (Figure 4h), which shows a generally positive correlation. It makes sense that higher C/N indicates higher exogenous OM input which may reflect more magnetic particles brought by terrigenous input. Figure S7 compares MSus, TOC, AL Ca and TD Mo/Mn records in Shira GC4 with the magnetic and OM records in Shira 2016 (Rogozin et al. 2016a) with depth. Both records show general agreements.

Paleoclimate and paleoenvironmental change over the past 200 years

The geochemical and elemental variation of the Lake Shira GC4 core can be categorized into six distinct zones:

- Zone I: 1870(?)–1900 CE (30–24 cm depth). During this period, lake level was high, with low productivity, salinity and alkalinity. Relatively high terrigenous input from surface runoff to the lake resulted in low organic matter but high AR elemental concentrations, reflecting warm and wet climatic conditions. At the end of this stage (ca. 1900 CE), Lake Shira was deep and relatively fresh with strongly reduced terrestrial input shown by all low parameters (Figures 4 and S5). This strong drop in terrestrial input may be a sign of drought condition which caused the lake level decline.
- Zone II: 1900–1940 CE (24–17 cm). Dry climatic conditions led to a drop in lake level, with elevated salinity and alkalinity. Lake level decreased by about 7 m from 1890 CE to 1930 CE (Figure S6). With increased salinity and alkalinity, carbonates deposited to form a white zone shown by high Ca, Sr and Mg contents, and a low magnetic signal. As carbonates precipitated in the lake sediments, alkaline earth and other elements were scavenged from the water column. This reduced the density and salinity of the lake water. Around 1925–1930 CE, the lake became holomictic and oxic as lake stratification diminished. The well-mixed water column increased the supply of nutrients and sunlight to enhance lake productivity. A slightly increased TOC trend in this zone supports this scenario. From 1930 CE to 1940 CE, the lake level gradually increased, and lake salinity decreased with elevated surface runoff. However, carbonate precipitation strongly decreased after 1940 CE.
- Zone III: 1940–1963 CE (17–13 cm). This zone marks a period of lake water stratification due to relatively high freshwater input during 1930–1940 CE. Anoxic conditions of deep lake water increased gradually since 1940 CE and reached a maximum around 1950 CE when the lake level was stable with reduced surface runoff, shown by low elemental contents with high Mo/Mn (Figures 4 and S6). Continuously increased TOC and C/N reflect an anaerobic and meromictic lake stage. An okenone-rich layer formed above the white carbonate zone as biogenic pigments were produced throughout anoxygenic photosynthesis in the lake bottom (Figures S6 and S7) (Rogozin et al. 2010, 2020; Zykov et al. 2012). The okenone formation led to enhanced OCI for ^{14}C dating of organic carbon.
- Zone IV: 1963–1994 CE (13–6 cm). The lake in this period had increased lake level with relatively high surface runoff (relatively high C/N, AR Fe, Al, Mn and MSus). The lake was relatively fresh (low AL Ca, Mg, Sr) in the early period, but its salinity increased in the later period shown by increased AL Ca. The lake became a relatively reduced environment and increased lake productivity after 1986 CE. The climatic condition was probably warming and wet.

- Zone V: 1994–2003 CE (6-4 cm). Lake Shira had a saline, meromictic, anoxic water column with high lake productivity, shown by relatively high AL Ca but a drop in other elemental fractions, high OM and Mo contents. The anaerobic and meromictic lake conditions favored of biogenic pigment formation (Figures S6 and S7).
- Zone VI: 2003–2020 CE (4–0 cm). The uppermost 3 cm of the sediments show high heavy metals (Pb, Cu, Zn, Cr, Ni) signifying anthropogenic impact after industrial development. The elevated OM and drop in C/N reflect increased lake productivity with more endogenous OM, implying eutrophication.

The description of the lake's history over the past 200 years shows a response to changes in climate conditions. Figures S6 and S7 provide a comparison of the lake records with their chronologies. In Figure S6, the comparison of Ca and Sr in Shira GC4 with the measured lake salinity shows a 5–10-year lag in the upper 15 cm (after 1950 CE). The cause of such a discrepancy is probably due to variations in sedimentation rate and lost surface sediments during coring. In Figure S7, the comparison of Shira GC4 with Shira 2016 (Rogozin et al. 2016a) indicates that the chronologies of both cores are comparable, but with a large difference below the white carbonate zone. In Shira GC4, 6 cm thickness accounts for 30 years below the white carbonate zone, whereas in Shira 2016 core 30 years deposited 1–2 cm thickness. Therefore, lamination counting results from a zone may not apply for different cores, and neither for different zones in the same core. Absolute dating methods such as ^{14}C dating should be utilized in the future. However, if a lake is impacted by old carbon influence, then the combined multi-proxy investigation with geochemical analyses is the best possible approach.

Conclusions

AMS ^{14}C dating on lake sediment TOC may account for OCI which could not be eliminated with ABA treatment. In addition, biogenic pigments in the lake sediments can have strong OCI in ^{14}C dating. The best way to solve this problem is to increase dating resolution and utilize the selected least OCI dates for age-depth construction. The OCI in the ^{14}C age of sedimentary TOC can be attributed to (1) aquatic submerged plants and algae using dissolved CO_2 which contains old carbon (reservoir effect) for photosynthesis; (2) reworked TOC from surface runoff; and (3) pigments such as Carotenoids formed by the photosynthesis of anoxic bacteria at the bottom lake. ABA treatment is not able to remove the above OCI from the TOC. However, the OCI varies with time under different lake conditions, being the least under low salinity and holomictic conditions. Thus, high-resolution dating will help in determining the ^{14}C age with the least OCI.

Using elemental geochemical proxies, it is better to separate them into 0.5N HCl acid leach (AL) and Aqua Regia total dissolution (AR) fractions. The AL fraction reflects mainly the influence of lake chemical conditions, whereas the AR fraction represents more terrigenous input with surface runoff and atmospheric fallout. AL Ca, Sr and Mg are indicators of lake salinity, alkalinity and pH. AL Mo, Mn, Fe, and Al are indicators of the redox condition of the lake. TOC%, TON% and C/N are proxies for lake productivity. Cu, Zn and Pb concentrations may be used for detecting human impact.

The Shira GC4 record shows climate and environmental changes over the past 200 years as follows: warm and wet climatic conditions during 1870~1900 CE but cool and dry during 1900~1940 CE. Lake Shira was saline, holomictic and oxic during 1900~1940. The lake became stratified and even meromictic with moderate productivity during 1940~1963 CE. Both salinity and productivity of the lake have increased from 1963 to 2000 CE. The lake became saline and meromictic conditions with anoxic deep water during 1994~2003. Since then, Lake Shira has decreased salinity with increased lake level. Human impact and industrial pollution have been recorded in the lake sediments.

References

Agatova AR, Nazarov AN, Nepop RK and Rodnight H (2012) Holocene glacier fluctuations and climate changes in the southeastern part of the Russian Altai (South Siberia) based on a radiocarbon chronology. *Quaternary Science Reviews* **43**, 74–93.

Andreev AA, Pierau R, Kalugin IA, Daryin AV, Smolyaninova LG and Diekmann B (2007) Environmental changes in the northern Altai during the last millennium documented in Lake Teletskoye pollen record. *Quaternary Research* **67**, 394–399.

Appleby PG and Oldfield F (1992) Application of lead-210 to sedimentation studies. In Ivanovich M and Harmon RS (eds), *Uranium-series Disequilibria. Applications to Earth, Marine, and Environmental Sciences*, 2nd edn. Oxford UK: Clarendon, 731–778.

Baskaran M, Bianchi TS and Filley TR (2017) Inconsistencies between ^{14}C and short-lived radionuclides-based sediment accumulation rates: Effects of long-term remineralization. *Journal of Environmental Radioactivity* **174**, 10–16.

Barkhatov YV, Khromechek EB, Zykov VV and Rogozin DY (2022. Cryptophytes of Lake Shira (Khakassia, Russia): Explosive growth during breakdown of meromixis. *Hydrobiologia* **849**, 3373–3387.

Belolipetsky PV, Belolipetskii VM, Genova SN and Mooij WM (2010) Numerical modelling of vertical stratification of Lake Shira in summer. *Aquatic Ecology* **44**, 561–570.

Belolipetskii VM, Degermendzhi AG, Genova SN and Rogozin DY (2017) Change in the circulation regime in the stratified saline Lake Shira (Siberia, Republic of Khakassia). *Doklady Earth Sciences* **474**(2), 649–652.

Björck J, Andrén T, Wastegård S, Possnert G and Schoning K (2002) An event stratigraphy for the Last Glacial-Holocene transition in eastern middle Sweden: Results from investigations of varved clay and terrestrial sequences. *Quaternary Science Reviews* **21**, 1489–1501.

Blaauw M and Christen JA (2011) Flexible paleoclimate age-depth models using an autoregressive gamma process. *Bayesian Analysis* **6**(3), 457–474.

Blyakharchuk T, Eirikh A, Mitrofanova E, Li HC and Kang SC (2017) High resolution palaeoecological records for climatic and environmental changes during the last 1350 years from Manzherok Lake, western foothills of the Altai Mountains, Russia. *Quaternary International* **447**, 59–74.

Blyakharchuk T, Udachin V, Li HC and Kang SC (2020) AMS ^{14}C dating problem and high-resolution geochemical record in Manzherok Lake sediment core from Siberia: Climatic and environmental reconstruction for northwest Altai over the past 1,500 years. *Frontiers in Earth Science* 8. https://doi.org/10.3389/feart.2020.00206.

Blyakharchuk T, Wright HE, Borodavko PS, van der Knaap WO and Ammann B (2004) Late Glacial and Holocene vegetational changes on the Ulagan high-mountain plateau, Altai Mountains, southern Siberia. *Palaeogeography, Palaeoclimatology, Palaeoecology* **209**(1–4), 259–279.

Blyakharchuk T, Wright HE, Borodavko PS, van der Knaap WO and Ammann B (2007) Late Glacial and Holocene vegetational history of the Altai Mountains (southwestern Tuva Republic, Siberia). *Palaeogeography, Palaeoclimatology, Palaeoecology* **245**(3–4), 518–534.

Blyakharchuk T, Wright HE, Borodavko PS, van der Knaap WO and Ammann B (2008) The role of Pingos in the development of the Dzhangyskol lake-Pingo complex, central Altai Mountains, southern Siberia. *Palaeogeography, Palaeoclimatology, Palaeoecology* **254**, 404–420.

Chappell A (1999) The limitations of using ^{137}Cs for estimating soil redistribution in semi-arid environments. *Geomorphology* **29**, 135–152.

Chen B, Zhao M, Yan H, Yang R, Li HC and Hammond DE (2021) Tracing source and transformation of carbon in an epikarst spring-pond system by dual carbon isotopes (^{13}C–^{14}C): Evidence of dissolved CO_2 uptake as a carbon sink. *Journal of Hydrology* **593**, 125766.

Chen FH, Huang XZ, Zhang JW, Holmes JA and Chen JH (2006) Humid little ice age in arid Central Asia documented by Bosten Lake, Xinjiang, China. *Science in China Series D: Earth Sciences* **49**, 1280–1290.

Chen JH, Chen FH, Feng S, Huang W, Liu JB and Zhou AF (2015) Hydroclimatic changes in China and surroundings during the medieval climate anomaly and Little ice age: spatial patterns and possible mechanisms. *Quaternary Science Reviews* **107**, 98–111.

Crusius J, Calvert S, Pedersen T and Sage D (1996) Rhenium and molybdenum enrichments in sediments as indicators of oxic, suboxic and sulfidic conditions of deposition. *Earth and Planetary Science Letters* **145**(1–4), 65–78.

Dar'in AV, Kalugin IA, Maksimov MA, Rogozin DY, Rakshun YV, Darin FA and Sorokoletov DS (2015) Reconstructing the Levels of Lake Shira over the last 1500 years with an annual time scale based on data from X-ray fluorescence microanalysis using beams of synchrotron radiation. *Bulletin of the Russian Academy of Sciences. Physics* **79**(1), 126–130.

Dar'in AV, Kalugin IA, Maksimov MA, Tretyakov GA and Rakshun YaV (2013) Scanning X-ray fluorescence microanalysis of annual layers in samples of Lake Shira bottom sediments. *Bulletin of the Russian Academy of Sciences. Physics* **77**(2), 185–187.

Degermendzhy AG, Zadereev ES, Rogozin, DY, Prokopkin IG, Barkhatov YV, Tolomeev AP, Khromechek EB, Janse JH, Mooij WM and Gulati RD (2010) Vertical stratification of physical, chemical and biological components in two saline lakes Shira and Shunet (South Siberia, Russia). *Aquatic Ecology* **44**(3), 619–632.

Dobrovolsky VV (1999) Fine particles of soils as a factor of mass transfer of heavy minerals in the biosphere. *Soil Science* **11**, 1309–1317. In Russian.

Dulamsuren C, Khishigjargal M, Leuschner C and Hauck M (2014) Response of tree-ring width to climate warming and selective logging in larch forests of the Mongolian Altai. *Journal of Plant Ecology* **7**(1), 24–38.

Fedeneva IN and Dergacheva MI (2003) Paleosols as the basis of environmental reconstruction in Altai mountainous areas. *Quaternary International* **106–107**, 89–101.

Gälman V, Rydberg J, Sjostedt de Luna S, Bindler R and Renberg I (2008) Carbon and nitrogen loss rates during aging of lake sediment: Changes over 27 years studied in varved lake sediments. *Limnology and Oceanography* **53**(3), 1076–1082.

Ganyushkin D, Chistyakov K, Volkov I, Bantcev D, Kunaeva E, Brandova D, Raab G, Christl M and Egli M (2018) Palaeoclimate, glacier and treeline reconstruction based on geomorphic evidences in the Mongun-Taiga massif (southeastern Russian Altai) during the Late Pleistocene and Holocene. *Quaternary International* **470**, 26–37.

Genova S, Belolipetskii V, Rogozin D, Degermendzhy A and Mooij W (2010) A one-dimensional model of vertical stratification of Lake Shira focussed on winter conditions and ice cover. *Aquatic Ecology* **44**, 571–584.

Grunert J, Lehmkuhl F and Walther M (2000) Paleoclimatic evolution of the Uvs Nuur basin and adjacent areas (Western Mongolia). *Quaternary International* **65–66**, 171–192.

Hatté C, Pessenda LC, Lang A and Paterne M (2001) Development of accurate and reliable ^{14}C chronologies for loess deposits: application to the loess sequence of Nussloch (Rhine valley, Germany). *Radiocarbon* **43**, 611–618.

Hausmann S, Larocque-Tobler I, Richard PJH, Pienitz R, St-Onge G and Fye F (2011) Diatom-inferred wind activity at Lac du Sommet, southern Quebec, Canada: A multiproxy paleoclimate reconstruction based on diatoms, chironomids and pollen for the past 9500 years. *The Holocene* **21**, 925–938.

Herren PA, Eichler A, Machguth H, Papina T, Tobler L, Zapf A and Schwikowski M (2013) The onset of Neoglaciation 6000 years ago in western Mongolia revealed by an ice core from the Tsambagarav mountain range. *Quaternary Science Reviews* **69**, 59–68.

Hildebrandt S, Müller S, Kalugin IA, Dar'in AV, Wagner M, Rogozin DY and Tarasov PE (2015) Tracing the North Atlantic decadal-scale climate variability in a late Holocene pollen record from southern Siberia. *Palaeogeography, Palaeoclimatology, Palaeoecology* **426**, 75–84.

Hua Q, Barbetti M and Rakowski AZ (2013) Atmospheric radiocarbon for the period 1950–2010. *Radiocarbon* **55**(4), 2059–2072.

Hua Q, Barbetti M and Zoppi U (2004) Radiocarbon in annual tree rings from thailand during the pre-bomb period, AD 1938–1954. *Radiocarbon* **46**(2), 925–932.

Hua Q, Turnbull JC, Samtos GM, Rakowski AZ, Ancapichún S, Pol-Holz RD, Hammer S, Lehman SJ, Levin I, Miller JB, Palmer JG and Turney CSM (2022) Atmospheric radiocarbon for the period 1950–2019. *Radiocarbon* **64**(4), 723–745.

Huang X, Peng W, Rudaya N, Grimm EC, Chen X, Cao X, Zhang J, Pan X, Liu S, Chen C and Chen F (2018) Holocene vegetation and climate dynamics in the Altai Mountains and surrounding areas. *Geophysical Research Letters* **45**(13), 6628–6636.

Ivankin GA (1979) Physico-geographical sketch of the region of geological practices (Khakassia). *Tomsk: Tomsk Polytechnic University Publishing House* 92. In Russian.

Jiang S, Zhou X, Tu L, Luo W, Ding M, Zhu A, Liu X, Liu X, Zhang J and Shen Y (2022) Radiocarbon age offset of lake sediments from central eastern China modulated by both hydroclimate and human activity. *Quaternary Science Reviews* **293**, 107726

Kalacheva GS, Gubanov VG, Gribovskaya IV, Gladchenko IA, Zinenko GK and Savitsky SV (2002) Chemical analysis of Lake Shira water (1997–2000). *Aquatic Ecology* **36**(2), 123–141.

Kalugin I, Darin A, Rogozin D and Tretyakov G (2013) Seasonal and centennial cycles of carbonate mineralisation during the past 2500 years from varved sediment in Lake Shira, South Siberia. *Quaternary International* **290–291**, 245–252

Kalugin I, Daryin A, Smolyaninova L, Andreev A, Diekmann B and Khlystov O (2007) 800-yr-long records of annual air temperature and precipitation over southern Siberia inferred from Teletskoye Lake sediments. *Quaternary Research* **67**(3), 400–410.

Kalugin I, Selegei V, Goldberg E and Seret G (2005) Rhythmic fine-grained sediment deposition in Lake Teletskoye, Altai, Siberia, in relation to regional climate change. *Quaternary International* **136**, 5–13.

Kaufman DS, Schneider DP, McKay NP, Ammann CM, Bradley RS, Briffa KR, Miller GH, Otto-Bliesner BL, Overpeck JT and Vinther BM (2009) Arctic lakes 2k project members. recent warming reverses long-term arctic cooling. *Science* **325**(5945), 1236–1239.

Kaushal S and Binford MW (1999) Relationship between C: N ratios of lake sediments, organic matter sources, and historical deforestation in Lake Pleasant, Massachusetts, USA. *Journal of Paleolimnology* **22**, 439–442.

Krylov PS, Nourgaliev DK and Yasonov PG (2015) Seismic investigations of Lake Chebarkul in the process of searching Chelyabinsk meteorite. *ARPN Journal of Engineering and Applied Sciences* **10**(2), 744–746.

Krylov P, Nurgaliev D and Yasonov P (2019) Seismic investigations of lakes sediments as the basis of paleogeographic and paleoclimatic reconstructions. *International Multidisciplinary Scientific GeoConference Surveying Geology and Mining Ecology Management, SGEM* **19**(1.1), 913–921.

Krylov PS, Nurgaliev DK, Yusopova AR, Sitdikov RN and Krylova AS (2022) Seismoacoustic Investigations of Lake Bolshoye Bele Bottom Sediments (The Republic of Khakasia, Russia). *ARPN Journal of Engineering and Applied Sciences* **17**(4), 504–508.

Lan B, Zhang D and Yang Y (2018) Lacustrine sediment chronology defined by ^{137}Cs, ^{210}Pb and ^{14}C and the hydrological evolution of Lake Ailike during 1901–2013, northern Xinjiang, China. *Catena* **161**, 104–112.

Le Roux G and Marshall WA (2010/2011) Constructing recent peat accumulation chronologies using atmospheric fall-out radionuclides. *Mires Peat* **7**, 1–14.

Li HC, Wang J, Sun JJ, Chou CY, Li HK, Xia YY, Zhao HY, Yang QN and Kashyap S (2019) Study of Jinchuan Mire in NE China I: AMS ^{14}C, ^{210}Pb and ^{137}Cs dating on peat cores. *Quaternary International* **528**, 9–17.

Li HC, Chang Y, Berelson WM, Zhao M, Misra S and Shen TT (2022) Interannual variations of D[14]C$_{TOC}$ and elemental contents in the laminated sediments of the Santa Barbara basin during the past 200 years. *Frontiers in Marine Science* **9**, 823793.

Meyers PA and Ishiwatari R (1993) Lacustrine organic geochemistry-an overview of indicators of organic matter sources and diagenesis in lake sediments. *Organic Geochemistry* **20**, 867–900.

Meyers PA (1997) Organic geochemical proxies of paleoceanographic, paleolimnologic, and paleoclimatic processes. *Organic Geochemistry* **27**, 213–250.

Meyers PA (2003) Applications of organic geochemistry to paleolimnological reconstructions: a summary of examples from the Laurentian Great Lakes. *Organic Geochemistry* **34**, 261–289.

Misra S, Kashyap S, Chou CY, Chang T, Li HC, Ning X, Sun JJ, Wang J and Zhao M (2024) The influence of plant species and pretreatment on the ^{14}C age of *Carex*-dominated peat plants of a peat core from Jinchuan Mire, NE China. *Radiocarbon*. Published online:1-21. doi:10.1017/RDC.2023.112.

Myglan VS, Oidupaa OC and Vaganov EA (2012) A 2367-year tree-ring chronology for the Altai-Sayan region (Mongun-Taiga Mountain Massif). *Archaeology, Ethnology and Anthropology of Eurasia* **40**(3), 76–83.

Ojala AEK, Saarnisto M, Jungner H, Snowball I and Muscheler R (2019) Biases in radiocarbon dating of organic fractions in sediments from meromictic and seasonally hypoxic lakes. *Bulletin of the Geological Society of Finland* **91**, 221–235.

Owen RB, Crossley R, Johnson TC, Tweddle D, Kornfield I, Davison S, Eccles DH and Engstrom DE (1990) Major low levels of Lake Malawi and their implications for speciation rates in cichlid fish. *Proceedings of the Royal Society B: Biological Sciences* **240**, 519–553.

Parnachev VP and Degermendzhy AG (2002) Geographical, geological and hydrochemical distribution of saline lakes in Khakasia, Southern Siberia. *Aquatic Ecology* **36**(2), 107–122.

Perdue EM and Koprivnjak JF (2007) Using the C/N ratio to estimate terrigenous inputs of organic matter to aquatic environments, Estuarine. *Coastal and Shelf Science* **73**(1–2), 65–72.

Reimer RW and Reimer PJ (2024) CALIBomb [www program] at http://calib.org assessed 2024-09-06. http://calib.org/CALIBomb/

Rogozin DY, Genova SV, Gulati RD and Degermendzhy AG (2010) Some generalisations on stratification and vertical mixing in meromictic Lake Shira, Russia, in the period 2002–2009. *Aquatic Ecology* **44**, 485–496.

Rogozin DY, Tarnovsky MO, Belolipetskii VM, Zykov VV, Zadereev ES, Tolomeev AP, Drobotov AV, Barkhatov YV, Gaevsky NA, Gorbaneva YB, Kolmakova AA and Degermendzhi AG (2017) Disturbance of meromixis in saline Lake Shira (Siberia, Russia): possible reasons and ecosystem response. *Limnologica* **66**, 12–23.

Rogozin DY, Zadereev E, Prokopkin I, Tolomeev A, Barkhatov Y, Khromechek E, Degermendzhi N, Drobotov A and Degermendzhi A (2016a) Chapter 5: Comparative Study of the Stability of Stratification and the Food Web Structure in the Meromictic Lakes Shira and Shunet (South Siberia, Russia). In RD Gulati, ES Zadereev and AG Degermendzhi (eds), *Ecology of Meromictic Lakes. Ecological Studies* 228, 89–124.

Rogozin DY, Zykov VV, Bulkhin AO and Degermendzhi AG (2020) Okenone in bottom sediments as a proxy for changes in the water level of a saline stratified lake. *Doklady Earth Sciences* **493**(1), 565–568.

Rogozin DY, Zykov VV and Tarnovsky MO (2016b) Dynamics of purple sulfur bacteria in saline meromictic Lake Shira (Khakasia, Siberia) for the period 2007–2013. *Microbiology (Russian Federation)* **85**(1), 93–101.

Routh J, Meyers PA, Gustafsson Ö, Baskaran M, Hallberg R and Schöldström A (2004) Sedimentary geochemical record of human-induced environmental changes in the Lake Brunnsviken watershed, Sweden. *Limnology and Oceanography* **49**(5), 1560–1569.

Rowan DJ, Kalff J and Rasmussen JB (1992) Profundal sediment organic content and physical character do not reflect lake trophic status, but rather reflect inorganic sedimentation and exposure. *Canadian Journal of Fisheries and Aquatic Sciences* **49**, 1431–1438

Rudaya N and Li HC (2013) A new approach for reconstruction of the Holocene climate in the Mongolian Altai: The high-resolution ^{13}C records of TOC and pollen complexes in Hoton-Nur Lake sediments. *Journal of Asian Earth Sciences* **69**, 185–195.

Rudaya N, Nazarova L, Novenko E, Andreev A, Kalugin I, Daryin A, Babich V, Li HC and Shilov P (2016) Quantitative reconstructions of mid- to late Holocene climate and vegetation in the north-eastern Altai Mountains recorded in Lake Teletskoye. *Global and Planetary Change* **141**, 12–24.

Saulnier-Talbot É, Pienitz R and Stafford Jr T (2009) Establishing Holocene sediment core chronologies for northern Ungava lakes, Canada, using humic acids (AMS ^{14}C) and [210]Pb. *Quaternary Geochronology*. **4**: 278–287.

Schlütz F and Lehmkuhl F (2007) Climatic change in the Russian Altai, southern Siberia, based on palynological and geomorphological results, with implications for climatic teleconnections and human history since the middle Holocene. *Vegetation History and Archaeobotany* **16**, 101–118.

Schubert CJ and Calvert SE (2001) Nitrogen and carbon isotopic composition of marine and terrestrial organic matter in Arctic ocean sediments: implications for nutrient utilization and organic matter composition. *Deep-Sea Research. Part I-Oceanography Research Paper* **48**, 789–810.

Schwikowski M, Eichler A, Kalugin I, Ovtchinnikov D and Papina T (2009) Past climate variability in the Altai. *PAGES News* **17**, 44–45.

Skurzyński J, Jary Z, Kenis P, Kubik R, Moska P, Raczyk J and Seul C (2020) Geochemistry and mineralogy of the Late Pleistocene loess-palaeosol sequence in Złota (near Sandomierz, Poland): Implications for weathering, sedimentary recycling and provenance. *Geoderma* **375**, 114459.

Smol JP and Cumming BF (2000) Tracking long-term changes in climate using algal indicators in lake sediments. *Journal of Phycology* **36**, 986–1011.

Stuiver M, Reimer PJ and Braziunas TF (1998) High-Precision Radiocarbon Age Calibration for Terrestrial and Marine Samples. *Radiocarbon* **40**(3), 1127–1151.

Sun A, Feng Z, Ran M and Zhang C (2013) Pollen-recorded bioclimatic variations of the last ∼22,600 years retrieved from Achit Nuur core in the western Mongolian Plateau. *Quaternary International* **311**, 36–43.

Tret'yakov GA, Kalugin IA, Dar'in AV, Rogozin DY and Degermendzhi AG (2012) Physicochemical conditions of seasonal carbonate precipitation in Shira Lake (Khakasia). *Doklady Earth Sciences* **446**(1), 1099–1101.

Unkelbach J, Dulamsuren C, Punsalpaamuu G, Saindovdon D and Behling H (2018) Late Holocene vegetation, climate, human and fire history of the forest-steppe ecosystem inferred from core G2-A in the 'Altai Tavan Bogd' conservation area in Mongolia. *Vegetation History and Archaeobotany* **27**, 665–677.

Vasilev BD and Parnachev VP (eds) (2006) *Geology and Mineralogy of North Khakasia (Guide to the educational geological site of universities in Siberia)*. Tomsk: Tomsk Polytechnic University Publishing House, 238 p. In Russian.

Westover KS, Fritz SC, Blyakharchuk TA and Wright HE (2006) Diatom paleolimnological record of the Holocene climatic and environmental change in the Altai mountains, Siberia. *Journal of Paleolimnology* **35**, 519–541.

Wilkins D, De Deckker P, Fifield LK, Gouramanis C and Olley J (2012) Comparative optical and radiocarbon dating of laminated Holocene sediments in two maar lakes: Lake Keilambete and Lake Gnotuk, south-western Victoria, Australia. *Quaternary Geochronology* **9**, 3–15.

Wittkop C, Bartley JK, Krueger R, Bouvier A, Georg RB and Knaeble AR (2020) Influence of provenance and transport process on the geochemistry and radiogenic (Hf, Nd, and Sr) isotopic composition of Pleistocene glacial sediments, Minnesota, USA. *Chemical Geology* **532**, 119390.

Yang S, Luo Y, Li Q, Liu W, Chen Z and Liu L (2021) Comparisons of Topsoil Geochemical Elements from Northwest China and Eastern Tibetan Plateau Identify the Plateau Interior as Tibetan Dust Source. *Science of the Total Environment.* **798**: 149240.

Zhao W, Liu L, Chen J and Ji J (2019) Geochemical characterization of major elements in desert sediments and implications for the Chinese loess source. *Science China Earth Sciences* **62**, 1428–1440.

Zhou W, Chui Y, Yang L, Cheng P, Chen N, Ming G, Hu Y, Li W and Lu X (2021) ^{14}C geochronology and radiocarbon reservoir effect of reviewed lakes study in China. *Radiocarbon* **64**(4), 833–844.

Zotina TA, Tolomeyev AP and Degermendzhy NN (1999) Lake Shira, a Siberian Salt Lake: ecosystem structure and function. 1. Major physico-chemical and biological features. *International Journal of Salt Lake Research* **8**(3), 211–232.

Zykov VV, Rogozin DY, Kalugin IA, Dar'in AV and Degermendzhi AG (2012) Carotenoids in bottom sediments of Lake Shira as a paleoindicator for reconstruction of lake states in Khakassiya, Russia. *Contemporary Problems of Ecology* **5**(4), 434–442.